Mustafa Böyük
DESIGNING A SYSTEM TO MANIPULATE MICRO MAGNETIC BEADS AND CELLSTHESIS TITLE
AGU 2018

DESIGNING A SYSTEM TO MANIPULATE MICRO MAGNETIC BEADS AND CELLS

A THESIS
SUBMITTED TO THE DEPARTMENT OF ELECTRICAL AND COMPUTER ENGINEERING
AND THE GRADUATE SCHOOL OF ENGINEERING AND SCIENCE
OF ABDULLAH GUL UNIVERSITY
IN PARTIAL FULFILLMENT OF THE REQUIREMENTS
FOR THE DEGREE OF
MASTER'S

By
Mustafa Böyük
December 2018

DESIGNING A SYSTEM TO MANIPULATE MICRO MAGNETIC BEADS AND CELLS

A THESIS
SUBMITTED TO THE DEPARTMENT OF ELECTRICAL AND COMPUTER ENGINEERING
AND THE GRADUATE SCHOOL OF ENGINEERING AND SCIENCE OF ABDULLAH GUL UNIVERSITY
IN PARTIAL FULFILLMENT OF THE REQUIREMENTS
FOR THE DEGREE OF
MASTER'S

By
Mustafa Böyük
December 2018

SCIENTIFIC ETHICS COMPLIANCE

I hereby declare that all information in this document has been obtained in accordance with academic rules and ethical conduct. I also declare that, as required by these rules and conduct, I have fully cited and referenced all materials and results that are not original to this work.

Mustafa Böyük

REGULATORY COMPLIANCE

M.Sc. thesis titled **"DESIGNING A SYSTEM TO MANIPULATE MICRO MAGNETIC BEADS AND CELLS"** has been prepared in accordance with the Thesis Writing Guidelines of the Abdullah Gül University, Graduate School of Engineering & Science.

Prepared By	Advisors
Mustafa Böyük	Assoc. Prof. Kutay İçöz
	Assoc. Prof. Günyaz Ablay

Head of the Electrical and Computer Engineering Program
Prof. Dr. Çağrı GÜNGÖR

ACCEPTANCE AND APPROVAL

M.Sc. thesis titled **"DESIGNING A SYSTEM TO MANIPULATE MICRO MAGNETIC BEADS AND CELLS"** and prepared by Mustafa BÖYÜK has been accepted by the jury in the Electrical and Computer Engineering Graduate Program at Abdullah Gül University, Graduate School of Engineering & Science.

12 /12/2018

JURY:

Advisor : Assoc. Prof. Kutay İçöz …….

Co-Advisor : Assoc. Prof.Günyaz Ablay …….

Member : Assoc. Prof.Ayşegül Güven …….

Member : Assist. Prof. Dooyoung HAH …….

Member : Assist. Prof. B. Hakan Aksebzeci …….

APPROVAL:

The acceptance of this M.Sc. thesis has been approved by the decision of the Abdullah Gül University, Graduate School of Engineering & Science, Executive Board dated ….. /….. / …….. and numbered ……..……. .

…….. /…….. / ……..

Graduate School Dean

Prof. Dr. İrfan ALAN

ABSTRACT

DESIGNING A SYSTEM TO MANIPULATE MICRO MAGNETIC BEADS AND CELLS

Magnetic tweezers are able to manipulate cells or biomolecules for various applications and measurements. In this study, an electromagnetic micromanipulator is designed, modeled and controlled for single magnetic bead manipulations. Electromagnetic tweezers are capable of controlling micron sized superparamagnetic particles with the help of appropriate control mechanism. Magnetic particles can be functionalized with receptors in order to capture the target biomolecules, and conjugated particles can be moved to a certain place by using an external magnetic field. Magnetic monopole and magnetic circuit approaches are used to model the dynamic equation of the magnetic system. An offset current based feedback linearizing is devised to ensure wide range of movement conditions with zero steady-state error. Image based algorithm is developed in order to find the position of the single particle. Numerical simulations are carried out in order to validate the derived model and the control system. The designed magnetic system is able to apply magnetic forces in the range of 1-100 pN to control a magnetic particle of 1 to 10 micrometer of diameter with a current less than 1 A. The magnetic micromanipulator system can be used for single cell separation, and biosensor applications.

Mustafa Böyük
MSc. in Electrical and Computer Engineering Department
Supervisor: Assoc. Prof. Kutay İçöz , Assoc.Prof. Günyaz Ablay

December 2018

Keywords: *Micromanipulation, Magnetic Tweezers, Magnetic Force, Control, Modeling, Tracking.*

ÖZET

MİKRO MANYETİK PARÇACIK VE HÜCRELERİN MANİPÜLASYONUNA YÖNELİK SİSTEM TASARIMI

Manyetik cımbızlar çeşitli uygulamalar ve ölçümler için hücreleri veya biyomolekülleri manipüle edebilir. Tek moleküllü manipülasyonlar için bir elektromanyetik mikro manipülatör tasarlandı, modellendi ve kontrol edildi. Elektromanyetik cımbız mikron boyutlu süperparamanyetik parçacıkları uygun kontrol mekanizması yardımıyla kontrol edebilir. Bu parçacıklar, hedef biyomoleküllerin yakalanması için reseptörler ile fonksiyonel hale getirilebildiğinden dolayı yüklü partiküller harici bir manyetik alan kullanılarak belirli bir yere taşınabilirler. Manyetik tek kutup ve manyetik devre yaklaşımları, manyetik sistemin dinamik denklemini modellemek için bu çalışmada kullanıldı. Ofset akım tabanlı geri besleme ile doğrusallaştırma yaklaşımı bir kontrolör tasarlanarak, sıfır kararlı-durum hatasıyla geniş çalışma koşulları sağlandı. Tek parçacığın konumunu bulmak için görüntü tabanlı algoritma geliştirilmiştir. Türetilmiş model ve kontrol sistemini doğrulamak için sayısal simülasyonlar yapılır. Tasarlanan manyetik sistem, 1 ila 10 mikrometre çapındaki manyetik bir parçacığı 1 amperden az bir akımla kontrol etmek için 1-100 pN arasında kuvvet uygulayabilmektedir. Manyetik yönlendirici sistemi, tek hücre ayrımı, ve biyosensör gelişmeleri için kullanılabilir.

Elektrik ve Bilgisayar Mühendisliği Ana Bilim Dalı, Yüksek Lisans Programı
Tez Yöneticisi: Doç. Dr. Kutay İçöz, Doç.Dr. Günyaz Ablay
Aralık 2018

Anahtar kelimeler: Micro-manipülasyon, Manyetik Tutucu, Manyetik Kuvvet, Kontrol, Modelleme, Referans Takibi.

Acknowledgements

Firstly, I would like to express my sincere gratitude to my advisors Assoc. Prof. Kutay İçöz and Assoc. Prof. Günyaz Ablay for the continuous support of my MSc study and related research, for their patience, motivation, and immense knowledge. Their guidance helped me in all the time of research and writing of this thesis during my time at Abdullah Gül University. Also I would like to thank the members of the committee Assoc. Prof. Ayşegül Güven, Assist. Prof. Dooyoung HAH, and Assist, Prof. B. Hakan Aksebzeci for agreeing to take part in my thesis defense.

I would like to thank Ünal Akar for Cell culture and immunomagnetic bead preperation.

I would also like to thank the Scientific and Technological Research Council of Turkey (TÜBİTAK) for supporting my studies during my Master of Science education under project number 116E168.

I would also like to thank the Scientific and Technological Research Council of Turkey (TÜBİTAK) for supporting Leukemia cell experiments section 4.4 during my Master of Science education under project number 115E020.

Publications:

G. Ablay, M. Böyük, Y. Eroğlu, K. İçöz, "A horizontal magnetic tweezer for single molecule micromanipulations," International Symposium on Multidisciplinary Studies and Innovative Technologies (ISMSIT 2018), Ankara, Turkey, 2018.

G. Ablay, M. Böyük, Y. Eroğlu, K. İçöz, "Active control of magnetic particles with a horizontal magnetic tweezer," International Mediterranean Science and Engineering Congress (IMSEC 2018), Adana, Turkey, 2018.

M. Böyük, K. İçöz, G. Ablay, "Electromagnetic Micromanipulator Designs for Biological Species," International Eurasian Conference on Biological and Chemical Sciences (EURASIANBIOCHEM 2018), Ankara, Turkey, 2018.

M.A. Canlılar, F.T. Selim, A. Payas, M. Böyük, K. İçöz, G. Ablay, "Design of Magnetic Tweezers for Single Molecule Manipulation," International Conference on Materials Science Mechanical and Automation Engineering and Technology (IMSMATEC 2018), İzmir, Turkey, 2018.

M. Böyük, M.N. Hasan, G. Ablay, K. İçöz, "Nickel micro pads and columns for trapping immunomagnetic beads and captured leukemia cells", 2nd International Conference on Material Science and Technology in Cappadocia (IMSTEC 2017), Nevşehir, Turkey, 2017

G. Ablay, K. İçöz, M. Böyük, "Micromanipulation based on electromagnetic actuators," International Scientific and Vocational Studies Congress (BILMES2018), Nevşehir, Turkey, 2018.

G. Ablay, M. Böyük, K. İçöz, "Design, modeling, and control of a horizontal magnetic micromanipulator", Transactions of the Institute of Measurement and Control. (accepted, pp. 1-26, 2018.)

Table of Contents

List of Figures

List of Tables

I dedicate this thesis to the lady of my life

and my beloved family

Chapter 1

Introduction

In recent years the micromanipulation systems have become an important research area due to their effective application potentials in various fields. Different types of actuating systems including magnetic, optical and atomic force microscopy based methods are designed for manipulation of micro particles. Firstly permanent magnet based magnetic tweezer was developed in order to manipulate DNA molecules conjugated with paramagnetic beads [1]. Permanent magnet based system can apply approximately 200 pN forces. Apart from the magnetic tweezer, optical tweezers are also used to trap magnetic particles in the cell biology [2]. Optical tweezers are stable but heating and photodamage are very critical issues [3]. For single molecule manipulation, AFM (atomic force microscopy) based tweezers are developed for cell biology and DNA extracting [4]. The developed magnetic tweezers are based on permanent magnets and electromagnets for single cell/molecule manipulation. In this concept, single pole and multipole magnetic tweezers have been developed to perform different manipulation tasks. Single pole magnetic tweezers [5] can be used to attract magnetic particles in one dimension without any control. In order to improve force direction and maneuverability, two-pole tweezers are developed [6]. The design and setup have been changed due to the technological developments [7]. Nanoscale manipulations are achieved with micro-magnetic tweezers. Hexapole tweezers are designed and developed for 3-dimensional actuation [8]. Dielectric particles are also trapped by electronic nano-tweezers [9]. Magnetic tweezers are designed and employed to offer an insight into the

function and dynamics of biomolecules, for instance extracting properties of DNA, RNA, and polymerases [10].

Permanent magnets offer simple designs without any control method or motorized designs for spatial manipulations. Permanent magnet based tweezers can be used for developing biosensors [11]. The experiences on manipulations of MAGLEV trains with electromagnets have been modified recently for micromanipulation applications [12]. The main advantage of magnetic tweezers is that they can perform three-dimensional movements with the help of control mechanisms. When we compare to the permanent magnets, the magnetic tweezers produce lower magnetic forces and they can be incorporated with a, control algorithm thus, magnetic tweezers can be a more powerful for biomedical applications [13].

The electromagnetic tweezers must be designed quantitatively to predict forces on superparamagnetic particles. Therefore we carried out our analysis with FEMM and Comsol software for solving electromagnetic field problems. The FEM (finite element method) is one of the most effective numerical calculation methods for magnetostatic problems. By changing the geometry of the core, tip and coil configurations the optimum and effective designs are obtained by using Comsol Multiphysics.

Experimental setup of double magnetic tweezers was tested and the tracking performance is observed with effective configurations. Then the study extended to the quadrupole magnetic tweezers. For in vivo and in vitro applications, magnetic force is the most effective action for biological operations because it is the non-invasive method.

Aim of this project: Our goal is to transport a single magnetic particle conjugated with biological molecules to a target location in the reservoir with a full automatic control system. Therefore we focused on designing magnetic tweezers for manipulating magnetic particles.

This thesis study consists of five sections. The first section reveals the properties of magnetic particles and their application areas. Section two, gives information about fundamentals of magnetism and magnetic force modeling,

and section three, gives details of manufacturing steps and FEM (finite element method) simulations. The control results are presented in section 4, and conclusion and future prospects are provided in section five.

1.1 Magnetic Beads

Magnetic beads are commercially produced in different sizes ranging from 10 nm to 100 µm and are composed of iron oxide nanoparticles which are typically made of magnetite ($\boldsymbol{Fe_3O_4}$) or maghemite $\boldsymbol{(\gamma - Fe_2O_3)}$, and polymer matrix coatings as illustrated in Figure 1.1 [14]. They have different features that make them appealing in medicine. One of the most important features of magnetic beads is that they can be magnetized under an external magnetic field. These magnetic beads are coated by different coatings such as a polymer that makes it functional for biological purposes. There are different sizes of magnetic beads for different applications. Since they are magnetic they can be controlled or manipulated by an external magnetic field. This feature can be used when magnetic beads are located in the non-magnetic medium.

There are different types of magnetic beads available for practical applications such as superparamagnetic beads, and ferromagnetic beads. In this work, we used superparamagnetic beads since they exhibit a non-magnetic behavior in the absence of an external magnetic field, namely residual magnetization or hysteresis phenomenon does not occur. The total magnetic moment of each bead equals the sum of the individual particles moments. Furthermore, their relative permeability is as strong as ferromagnetic materials. Hence superparamagnetic particles are used applications in cell manipulation, DNA extracting, immunoassays, targeted medication, magnetic resonance imaging and hyperthermia therapies in medical applications as a powerful non-invasive tool [15].

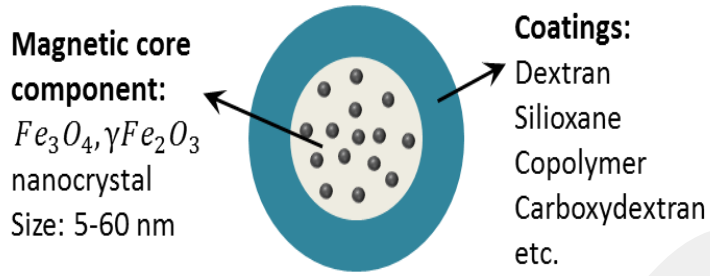

Figure 1.1 Structure of a superparamagnetic particle.

1.2 Application of Magnetic beads

There are many fields where the magnetic beads are used but the main applications of superparamagnetic particles are found in biomedical systems [16], for instance, antibody-coated, streptavidin-dextran coated, and fluorescence-coated magnetic particles are available for versatile applications.

1.2.1 Magnetic separation

Magnetic particles have been used for separation of cells or molecules since they are attracted to high magnetic flux density [17]. One of the most promising magnetic separation method is based on usage of antibodies conjugated with particles that can specifically bind to their matching agents on the surface of the targeted sites. The principle of the concept is based on application of external magnetic field on the labeled entities that will be separated from unlabeled entities. In this way, tumor cells, enzymes, and DNA/RNA can be removed from blood or medium.

1.2.2 Drug Delivery

The treatment of tumors have been achieved by using chemotherapy which results in harmful effects on the whole body since the drugs that are used in chemotherapy are not locally distributed to required areas hence magnetic

particles have been developed for localizing drug delivery to the tumor [18]. Magnetic nanoparticle serves as a drug carrier. The surface of the magnetic particle is functionalized with the drug and the drug coated magnetic particles are introduced into the bloodstream of the patient and then these particles are attracted at targeted region by applying external magnetic field. Finally, the drug is released via an enzymatic activity or a controlled triggering mechanism. The potential advantage of drug delivery is listed as follows. It targets the specific locations in the body, it leads to a decrease in the amount of drug concentration and it provides patients with less severe side effects.

1.2.3 Magnetic Resonance Image

The superparamagnetic nanoparticles can be used to enhance magnetic resonance imaging contrast [19]. The basic concept is that spinning protons have a magnetic moment. The application of a strong magnetic field causes movements of the protons to line up parallel to the magnetic field. Nuclear spins have two energy states, low-energy states where protons aligned parallel to the magnetic field and high-energy states where protons aligned to perpendicular to the magnetic field. The signal that is called Free Induction Decay produced as a result of this alignment is measured when the amplitudes of magnetic moments relax back to their initial values after the magnetic moment turned off. This signal is obtained from inductive coils. Since human body composed of a high amount of water which contains hydrogen and oxygen atoms, the magnetic resonance based images can be taken by rotating these hydrogen atoms applying an external strong magnetic field. Proton density and relaxation time effects the contrast of the image, therefore, magnetic nanoparticles are used to enhance the contrast of the image by reducing the relaxation time of protons.

1.2.4 Hyperthermia

Hyperthermia is a new and safe method used to treat cancerous tissues. This treatment is based on the killing of cancerous cells in the tissues. When a

high frequency (~1 MHz) field is applied, magnetic particles begin to rotate due to heat this leads to the death of cancerous cells. The upper limit of the temperature is chosen to be around $43^{o}\mathbf{C}$ to avoid damage to other cells in the tissue. While the heating mechanism for ferromagnetic materials can be explained by hysteresis losses, heating for superparamagnetic particles can be achieved by rotation of particles [20]. It is possible to apply magnetic particle heating at the depths necessary for the treatment of tumors located anywhere in the human body.

Chapter 2

Magnetism and Magnetic Force Modeling

There have been many different types of material in nature, i.e. all materials have different features. The common feature of these materials is that they have magnetic behavior. Their response against an external magnetic field changes from material to material. There is a strong relationship between magnetism and magnetic moment which is the source of magnetism. It is important to understand the magnetic behavior of materials. The basic concept of magnetism results from the rotating of electrons around the nucleus or around their own axes and the rotating of protons in the nucleus around their own axes. According to magnetic theory atomic magnetic moment consist of three sources;

1- Electrons spin angular momentum, that results from rotation of the electrons around its own axis.

2- Orbital angular momentum, which results from rotation of the electrons that located the farthest orbital of the atom around the nucleus.

3- Changes in angular momentum which results from an applied external magnetic field [21].

Magnetization is the response of electrons in a material when an external magnetic field is applied. All materials give various responses to the external magnetic field. Their behaviors determine their magnetic property. On the other hand, magnetic susceptibility χ determines the magnetic moment in the material. Magnetic field inside the material can be described as a function of the applied

magnetic field. All materials give various responses to the external magnetic field. Their behaviors determine their magnetic property.

2.1 Magnetism

The magnetic relation is defined by

$$B = \mu H \tag{2.1.1}$$

where μ is the permeability of the material, *B* and *H* refer to the magnetic flux density and the magnetic field intensity, respectively. The commonly used units in magnetism are illustrated in Table 2.1 for CGS and SI systems. When a material is subjected to an external magnetic field, a magnetization occurs defined as:

$$M = \chi H \tag{2.1.2}$$

where χ is the susceptibility of material and M is the magnetization(A/m) which can be written as

$$M = \frac{m}{V_b} \tag{2.1.3}$$

m and V_b refer to magnet moment and volume of material. By considering equation **(2.1.1)** and **(1.2.2)**, the final equation of magnetic flux density can be obtained by

$$B = \mu o(H + M) \tag{2.1.4}$$

where μo is the permeability of free space that equals to $4\pi \times 10^{-7}$ (in Tm/A) and the relationship between permeability and susceptibility of material can be described as:

$$\mu = \mu o(\chi + 1) \tag{2.1.5}$$

From equation (**2.1.5**) χ magnetic susceptibility is used to classify materials in presence of magnetic field. Materials can be classified as ferromagnets, ferrimagnets, paramagnets, diamagnets and antiferrimagnets due to their magnetic response. Applied magnetic field and temperature also have a curicial impact on the magnetic susceptibility of these materials.

Symbol	Description	CGS	SI
H	Magnetic Field Strength	Oe	A/m
B	Flux Density	Gauss	Tesla
φ	Flux	Maxwells	Webers
M	Magnetization	emu/cm3	A/m

Table 2.1 CGS and SI systems

2.2 Classification of Magnetic Materials

2.2.1 Diamagnetism

A diamagnetic material does not have a net magnetic moment in the absence of a magnetic field when an external magnetic field is applied, the molecules, even if small, have a magnetic moment. These magnetic moments of the molecules are induced by the external applied magnetic field. The induced magnetic moment aligns in the opposite direction to the applied magnetic field thus the magnetization of the particle occurs in the opposite direction to the magnetic field such materials are called diamagnetic [22]. Diamagnetic material acquires the opposite magnetization with the field regardless of the direction of the external magnetic field. Diamagnetism can be seen in substances that their orbitals are fully filled like noble gases. Since the magnitude of the force that pushes a diamagnetic material out of the field is very small, it is very difficult to observe the interaction of such materials with the magnetic field.

The susceptibility of diamagnetic materials is negative and ranging from -10^{-6} to -10^{-3}.

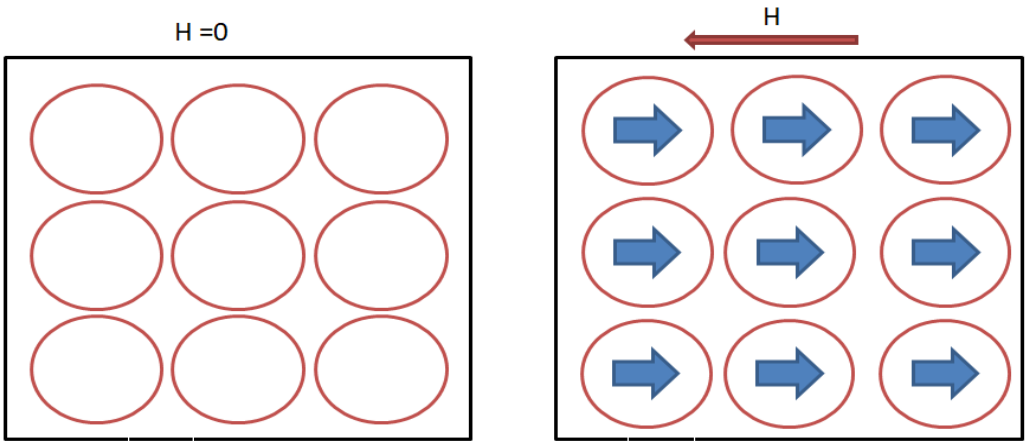

Figure 2.2.1.1 Magnetic moments of diamagnetic response of a material with (a) zero magnetic fields and (b) applied external magnetic field.

2.2.2 Paramagnetism

Paramagnetic material has net magnetic moment due to spin of the uncoupled electrons in molecular electron orbitals. In paramagnetic material, magnetic moments are randomly oriented in the absence of a magnetic field. When an external magnetic field is applied, magnetic moments align up the direction of the external magnetic field and then they will be randomly oriented in case of removal of the external magnetic field. Weak magnetism can be observed in paramagnetic materials which can have a range from 10^{-6} to 10^{-1}. As the strength of the applied external magnetic field is increased, the magnetization of the material increases accordingly. The susceptibility of these materials is dependent on temperature and is shown in the equation (2.2.2.1).

$$\chi = \frac{C}{T} \qquad \textbf{(2.2.2.1)}$$

where C is the Curie constant and T is the absolute temperature. Ferromagnetic material becomes paramagnetic behavior above the critical temperature which is known as Curie temperature. The relationship between susceptibility and temperature can be explained by Curie-Weiss equation [23].

$$\chi = \frac{C}{(T-T_c)} \qquad \textbf{(2.2.2.2)}$$

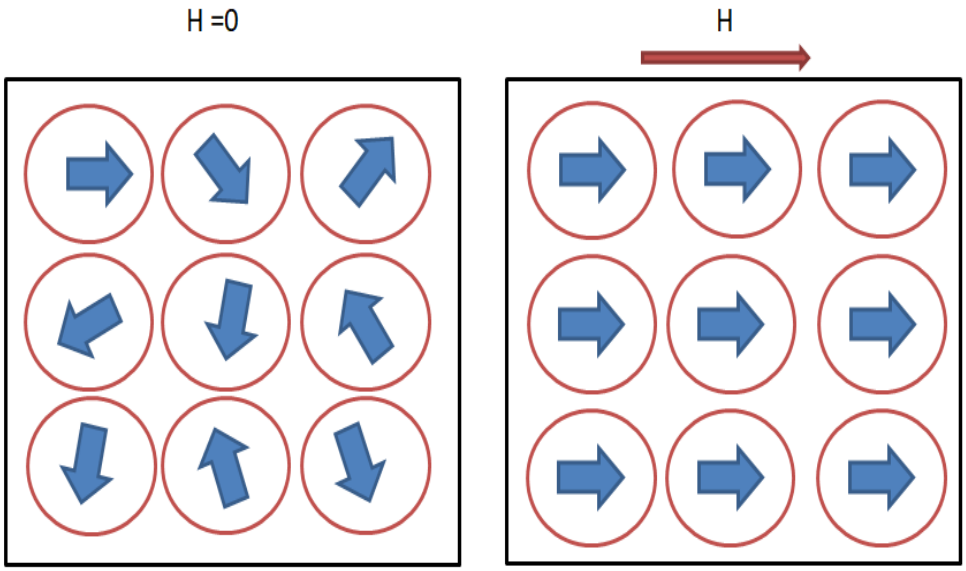

Figure 2.2.2.1 The arrows represent the magnetic moment of a paramagnetic material under the applied magnetic field.

2.2.3 Ferromagnetism

Ferromagnetism is only possible in cases where magnetic moments aligned parallel to each other. Magnetic moments have net magnetization even the absence of an external magnetic field. Ferromagnetic material has a small region called domain where all magnetic moments aligned in one direction [23]. Once a magnetic field is applied, all domains show parallel alignment in the direction of the magnetic field. These materials have a tendency to maintain their magnetization even the external magnetic field is removed. Ferromagnetism can be observed in certain temperature known as Curie temperature above this temperature material begins to behave paramagnetic. Ferromagnetic materials can reach saturation even in the very small magnetic field. Ferromagnetic materials can be classified into two categories of soft and hard ferromagnetic materials. To exemplify; iron is a soft ferromagnetic because

once it is magnetized, it does not show permanent magnetization after the removal of the external magnetic field.

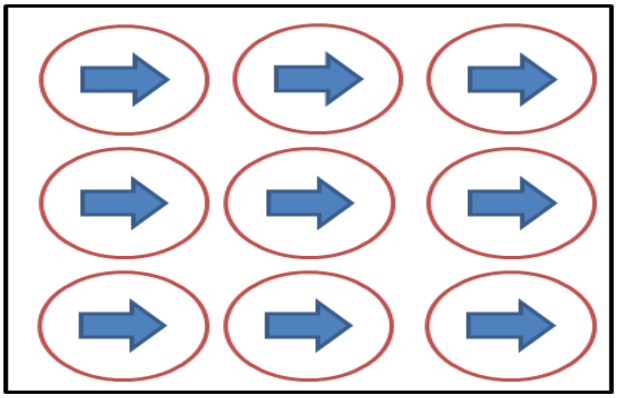

Figure 2.2.3.1 Magnetic moment of a ferromagnetic behavior with an external magnetic field.

2.2.4 Antiferromagnetism

In ferromagnetism, spin orientations are in the same direction while antiferromagnetic materials have opposite spin orientations. On the other hand, their magnetic moments align antiparallel to each other. They have zero net magnetization since these antiparallel aligned moments have the same magnitude. Hence they will cancel out each other. Antiferromagnetic materials show similar behavior with ferromagnetism at a certain temperature, their magnetic response varies above the Neel temperature [24].

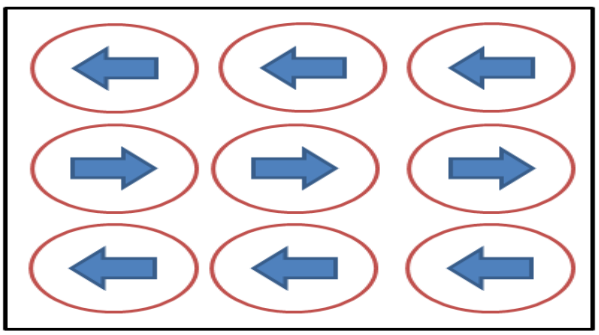

Figure 2.2.4.1 Anti-parallel magnetic moment of a material.

2.2.5 Ferrimagnetism

Similar to antiferromagnetic material, ferromagnetic materials have antiparallel magnetic moment alignment but their magnitude of the moments differ from each other therefore they cannot cancel each other and they show weak magnetic susceptibility.

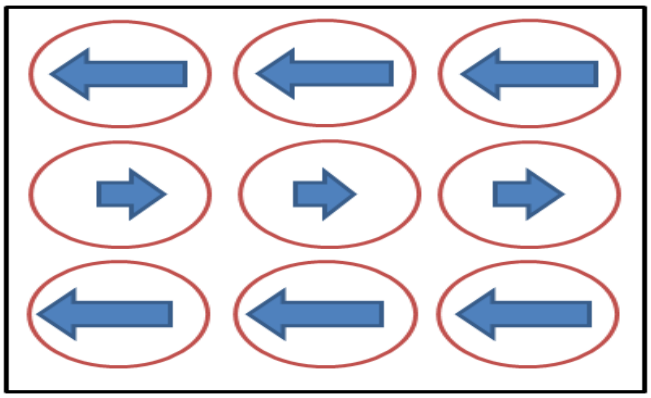

Figure 2.2.5.1 Magnetic moments of ferromagnetic material.

2.2.6 Superparamagnetism

Ferromagnetic and ferrimagnetic beads have a special property that is called superparamagnetism due to their small size which ranges from 100 µm to 10 µm. These beads have only one single domain hence they have a tendency to flip randomly due to the thermal energy. The typical time between two flips can be described by

$$\tau = \tau_o exp(\frac{\Delta E}{k_B T}) \qquad \textbf{(2.2.6.1)}$$

where τ_o is the relaxation time ΔE is the energy barrier $k_B T$ is the thermal energy. In order to observe superparamagnetism in the nanoparticles not only temperature and energy barrier but also needed measurement time, T_m should be required.

Similar to paramagnetism, when an external magnetic field is applied, they behave like paramagnet yet having greater magnetic susceptibility distinguish it from paramagnetism. A hysteresis loop shows the magnetic

response of a material between the induced magnetic flux density (B) and the magnetizing force (H) furthermore such a superparamagnetic material has no hysteresis loop. Magnetization equals to zero after the removal of magnetic field. M-H curve shown in Figure 2.2.6.1 [25].

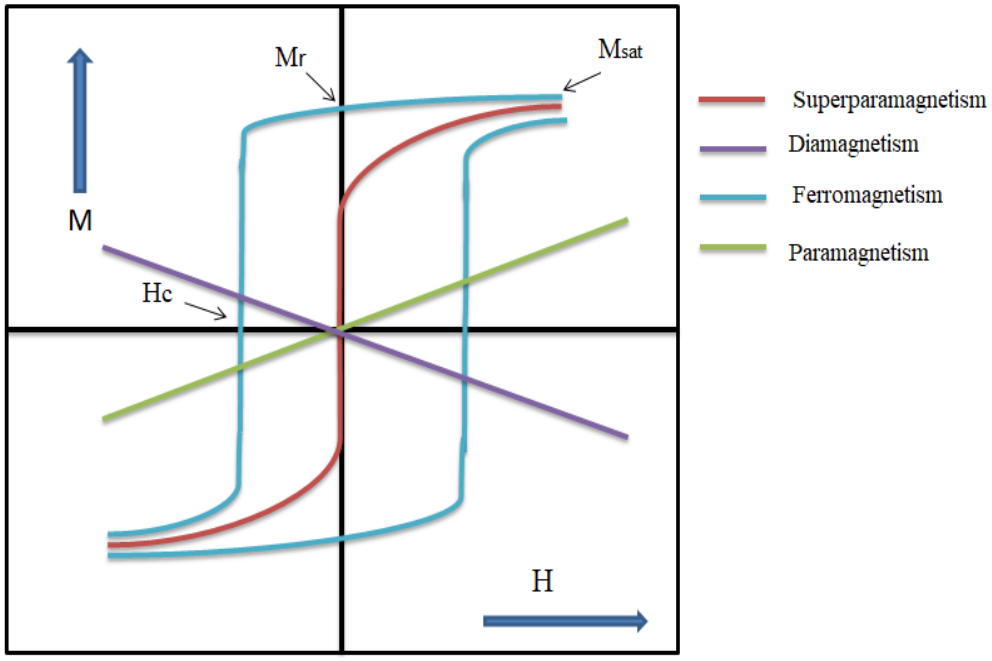

Figure 2.2.6.1 Para-dia-ferro magnetic behaviors and hysteresis loop of a ferromagnetic material.

Chapter 3

Materials and Methods

In this chapter, the magnetic system configuration, magnetic set-up, image based particle detection and magnetic flux density simulations are addressed. We determine to magnetic flux density on the surface of the tip and near the tip. The effects of length of the taper, tip radius, and core radius and selonoid positions have been studied in order to find optimum designs. Also, multi-pole magnetic tweezers concepts are studied.

3.1 Magnetic System Configuration

The geometry of core has a crucial role in magnetic field strength on the other hand core material has a strong impact on the strength of magnetic field. Large magnets generate strong magnetic fields and it provides a magnetic tweezer system with high force generated by a magnetic system on a bead. The magnetic actuating system consists of several parts: fluidic reservoir, electromagnet, core, microscope system, computer, control system and DC power supply. The electromagnets and fluidic reservoir system placed on plexiglass and electromagnets are fixed with plastic clamps. The core of electromagnets is made of steel for strong magnetic force generation. CNC machine is used to shape the geometry of the core. The shape of the tips has a crucial role in magnetic flux generation. Hence their shape and length are designed according to the radius of the working region to produce a uniform flux density. A camera-microscope system is used to detect magnetic particles

and its positions in the reservoir. 10X object is used for the image acquisition system. A motorized manipulator is used to adjust the position of micromanipulator and camera system in x-y-z directions. We used USB 2.0 CMOS industrial camera to detect magnetic particles. The image acquisition system can capture 53 frames per second with 640x480 pixel ^{2} resolution. The electromagnetic system is connected to a DC power supply to control currents. The fine motor resolution allows focusing on particles with different sizes. For data acquisition and processing, a workstation equipped with performance CPU and Matlab software is used. Particle detection and tracking system is developed in Matlab. A center of mass particle tracking algorithm and a threshold filter is used to separate the difference in brightness between the particle and background. Mosfet controlled current sources and microcontrollers are used to adjust the current sources and produce PWM signal. The tips are placed near the reservoir as close as possible. The radius of the working area is adjusted to be 2 mm. The important point is that when we extend the working area, high magnetic force is needed to move particles and it can lead to the saturation of material. Therefore iron, cobalt, and their alloys should be used for the highest magnetic saturation level.

The operation principle: to move the particle in one dimension two electromagnets on the same axes are needed, because the coils can only pull the microbeads. In order to move the particle in two dimensions four electromagnets needed which resulted in quadrupole design. The current of the electromagnet regulates the magnetic force generated by the coil. By applying more current the bead will move towards the coil that produces extra force than the other coil. The fluidic reservoir is made of Polymethyl methacrylate (PMMA) material. The geometry of fluidic reservoir is designed in CAD software and a double side of the PMMA is glued in order to avoid any leaking. A piece of PMMA is cut and shaped using a laser cutter (Epilog Zing 16). The reason why we fabricated fluidic reservoir from PMMA is that it shows quality optical properties, in terms of light transparency and the most important one is its biocompatibility to living cells.

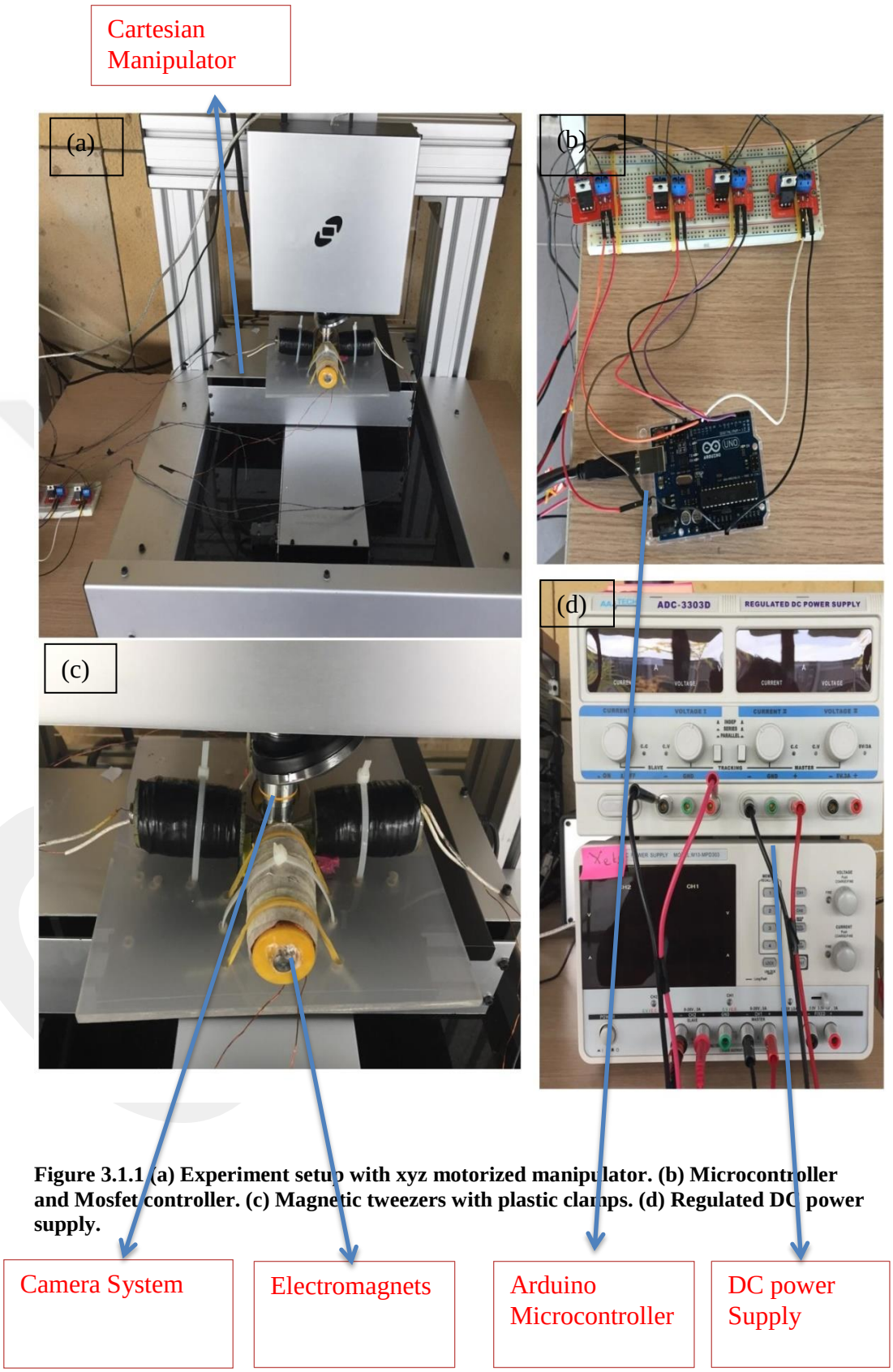

Figure 3.1.1 (a) Experiment setup with xyz motorized manipulator. (b) Microcontroller and Mosfet controller. (c) Magnetic tweezers with plastic clamps. (d) Regulated DC power supply.

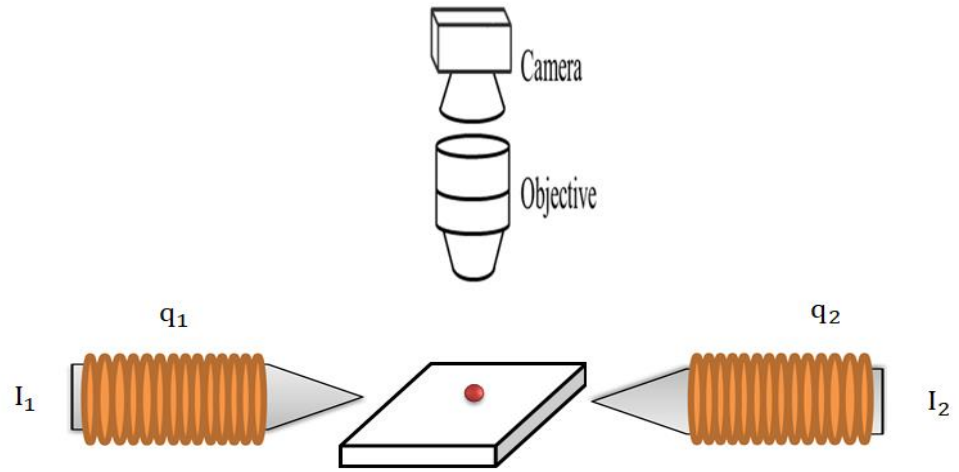

Figure 3.1.2 Schematic diagram of the magnetic tweezer.

3.1.1 Solenoid

In this study, the coil is made of copper wires wrapped on a cylindrical material. These cylindrical materials are produced by the 3D printer. Their role is to reduces the heat transmission and help to adjust the position of the magnetic core in the experiment. The coil consists of 2000 turns with diameter 0.455 mm copper wire.

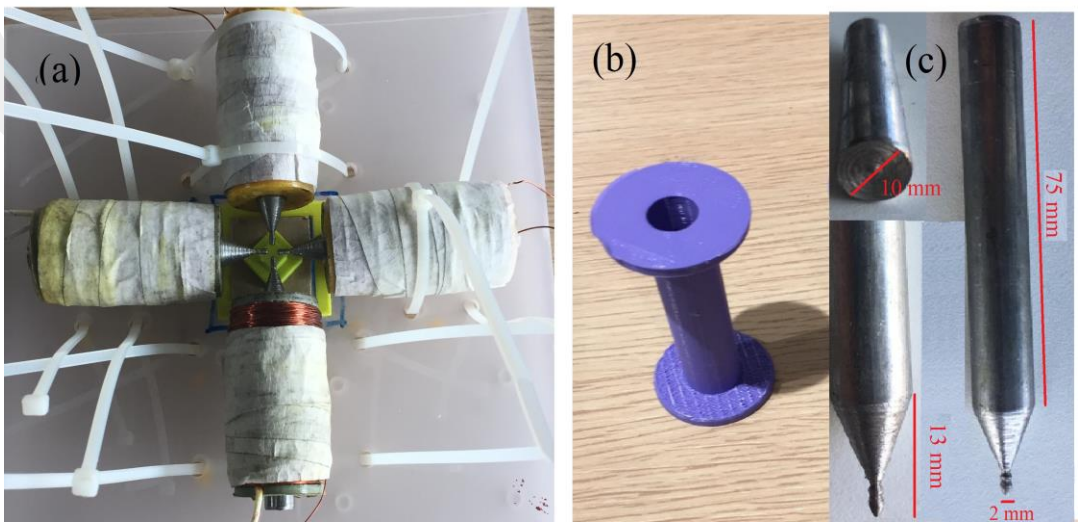

Figure 3.1.1.1 (a) Magnetic tweezer setup. (b) 3D printed tubes. (c) Steel Core.

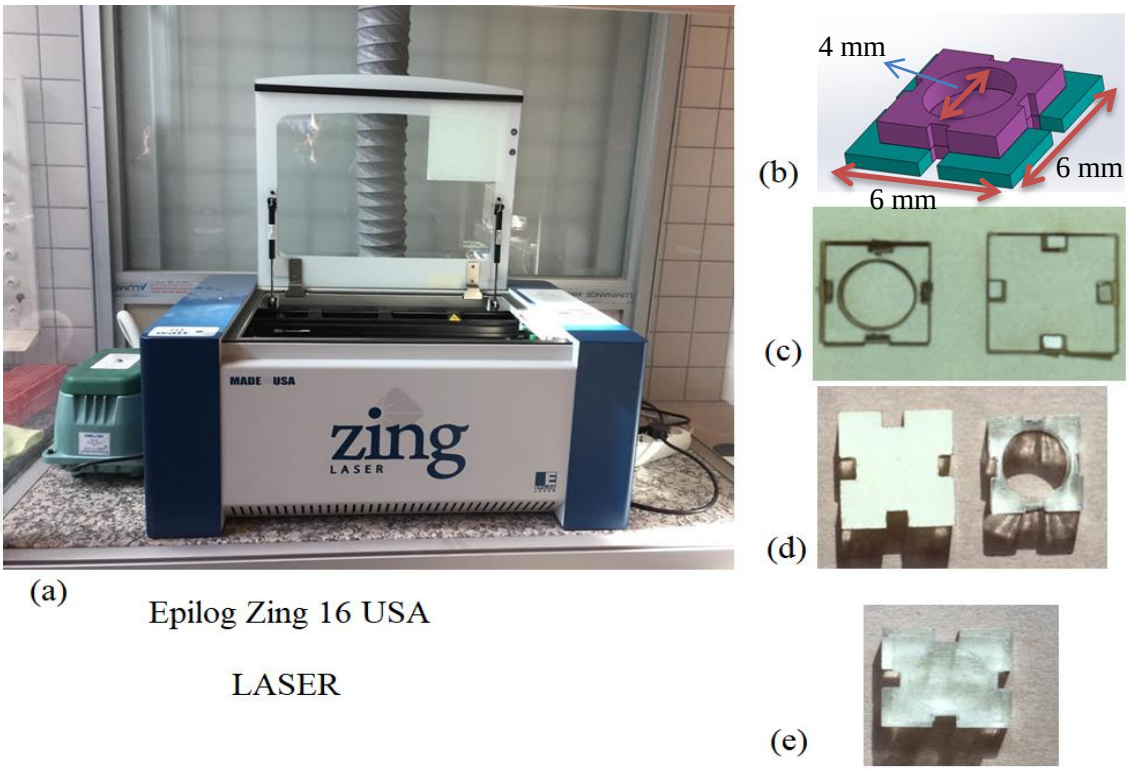

Figure 3.1.1.2 (a) Laser Cutting Machine and ventilation system, (b) CAD design of fluidic reservoir, (c), (d) The fluidic system after laser cutting, (e) Final Setup.

The microfluidic reservoir has 2 mm height and 2 mm radius with circular shape and it is made of PMMA glass which is suitable for biological molecules.

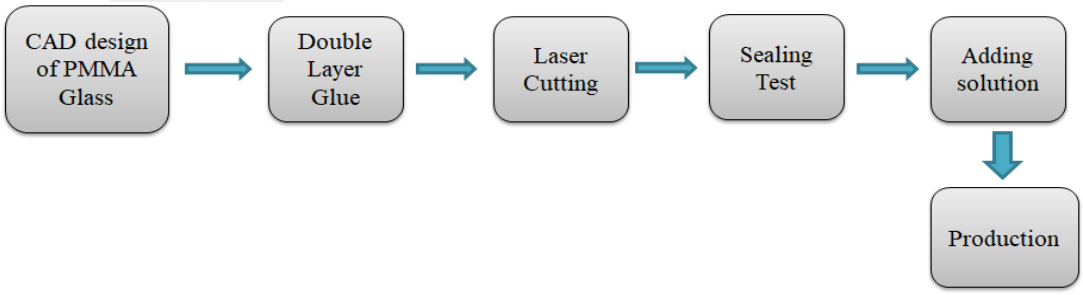

Figure 3.1.1.3 Fluidic reservoir design steps.

3.1.2 Image Based Magnetic Particle Detection

For experimental studies, the magnetic particle in a liquid workspace is detected and tracked by using a Matlab based image processing algorithm as illustrated in Figure 3.1.2.1. A color image frame is captured from the video, and then it is converted into grayscale and binary images using some threshold values. The connectivity information of the particles in the binary image is used to detect the circular objects. Finally, the pixels of the detected particles are determined and converted into position values for use in the control designs. The connected pixels are neighbors to every pixel that touches the one of their edges or corners.

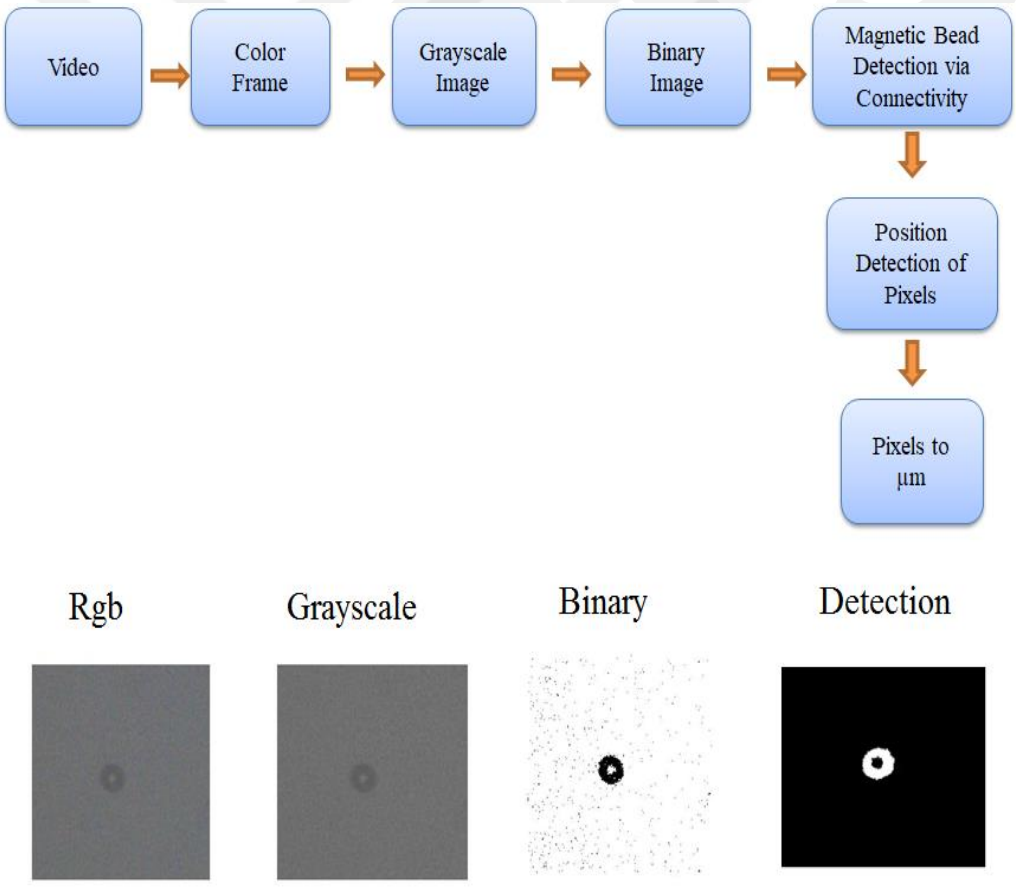

Figure 3.1.2.1 Image based magnetic particle detection algorithm.

3.2 Design of Electromagnets Using Comsol

Comsol Multiphysics software is a simulation platform that solves numerical problems and enables powerful solutions for problems. It is designed to simulate real-world physical systems and to optimize these systems with simulation. Comsol provides engineers with quicker and more efficient and accurate optimization process due to the ability to solve partial differential equations. Comsol allows users to select related fields to solve physical problems and includes Electromagnetics, Diffusion, Fluid Dynamics, RF module Chemical module. In this work, the magnetostatic problem of the magnetic tweezers is solved by using the finite element method with Comsol. Analytical methods including Biot-Savart law may be implemented to get solutions but the complexity of geometry and usage of different materials makes such an analytical solution cumbersome. We utilize Comsol Multiphysics for two, axisymmetric and three dimensional solutions. Since the three dimensional model requires high computation effort and time, the axisymmetric 2D model is used to get solutions in AC/DC model. The software utilizes the Maxwell equation defined below to solve magnetostatic problems,

$$B = \nabla \times A \quad , \quad \nabla \times H = J \tag{3.2.1}$$

where A is the magnetic vector potential, J is the current density and defined by

$$J = \sigma_c E + J_e \quad , \quad J_e = N I_{coil} / A_{coil} \tag{3.2.2}$$

where E is the electric field intensity, σ_c is the electrical conductivity , N is the number of turns in the coil, I_{coil} is the total coil current, and A_{coil} is the total cross section area of the coil domain. Comsol computes the magnetic field B and its component in a region of interest, which can be exported from the program. Electromagnetic tweezers are simulated and magnetic flux density is calculated according to the Maxwell stress tensor method which is defined in **(3.2.1)** and **(3.2.2)**.

3.2.1 Comsol Modeling

To obtain simulation analysis we must follow some steps to solve problems in Comsol Simulation flow follow required steps as adding magnetic field interface block and study type, creating geometry for analysis, building geometry with desired materials and properties, adding boundary conditions, meshing the defined geometry and working region and visualization of results.

3.2.2 Geometry

Many electromagnets are designed quantitatively to find optimum coil shape, taper length, and core radii. Figure 3.2.2.1 shows the model geometry.

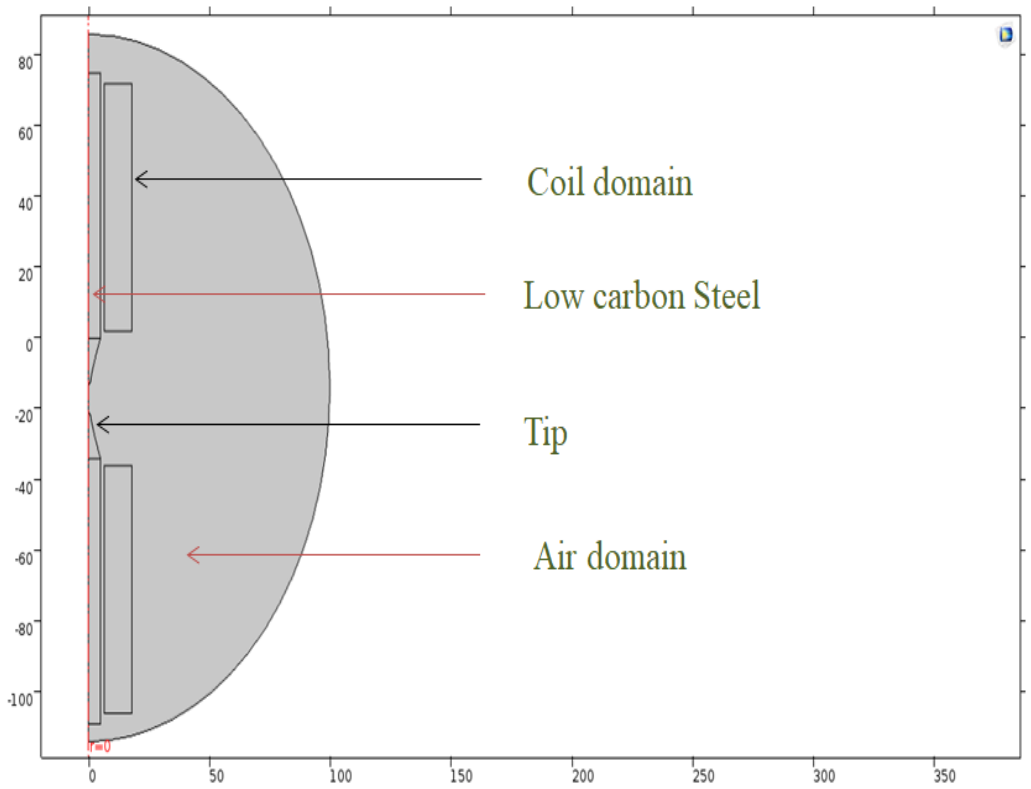

Figure 3.2.2.1 Geometry of horizontal magnetic tweezers.

3.2.3 Meshing

Meshing process is very important for Finite element analyses for getting accurate solutions. Hence in the solution of tweezer designs, extremely fine element size is chosen for the tip to get precise solutions. On the other hand, air and coil meshes are selected much coarser than core domain during the simulation process.

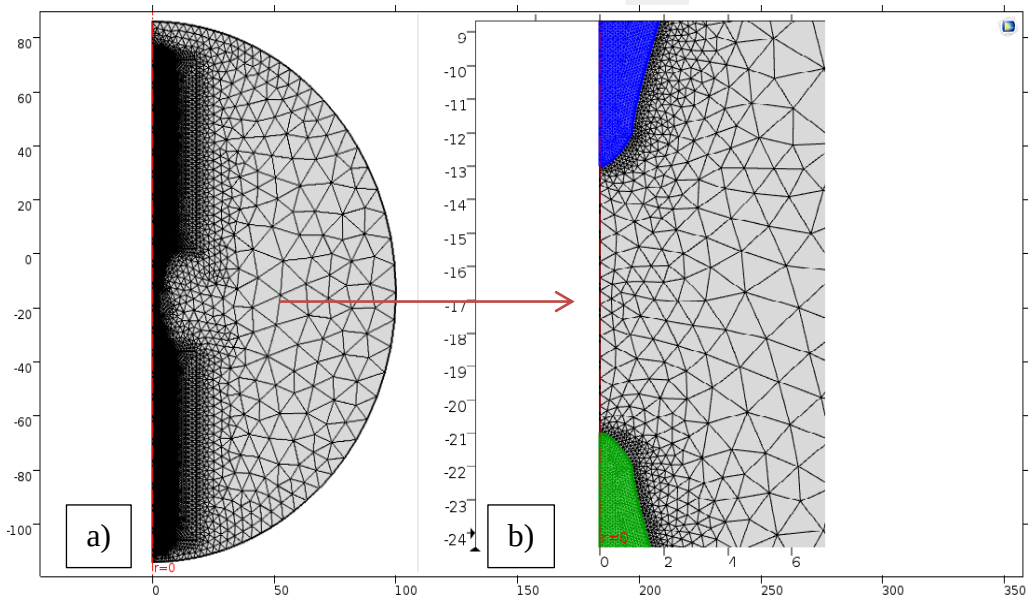

Figure 3.2.3.1 Extremely fine (a) and coarse meshing domains (b) closer look at the apex of the tip.

3.3 Magnetic flux density simulations

The magnetic flux density generated by the electromagnet is depended on several factors including core diameter, core length, tip radius, taper length, solenoid current, solenoid position, and permeability of the material. It is obvious that all combinations cannot be done experimentally, because such a work requires a high amount of cost and time. To reduce experiment time we used finite element method to obtain effective configurations.

3.3.1 The effect of tip radius

Figure 3.3.1.1 shows that the magnetic flux density changes along the z-axis. Magnetic tip radius changes from 0.05 to 0.1 mm. The sharp edges of tip were smoothed in order to obtain accurate simulation results. The sharper the tip is, the higher magnetic flux density will be. According to simulation results, the highest magnetic flux density is obtained in the vicinity of the tip when tip radius is 0.05 mm. Yet flux density along the 1 mm decreases very fast.
Hence the distance for 1 mm, light blue line represents 1 mm tip radius gives the highest magnetic flux density. Another important point is that when the tip gets sharper, the flux density which is produced by electromagnet becomes non-uniform and the controllability of magnetic beads becomes more difficult.

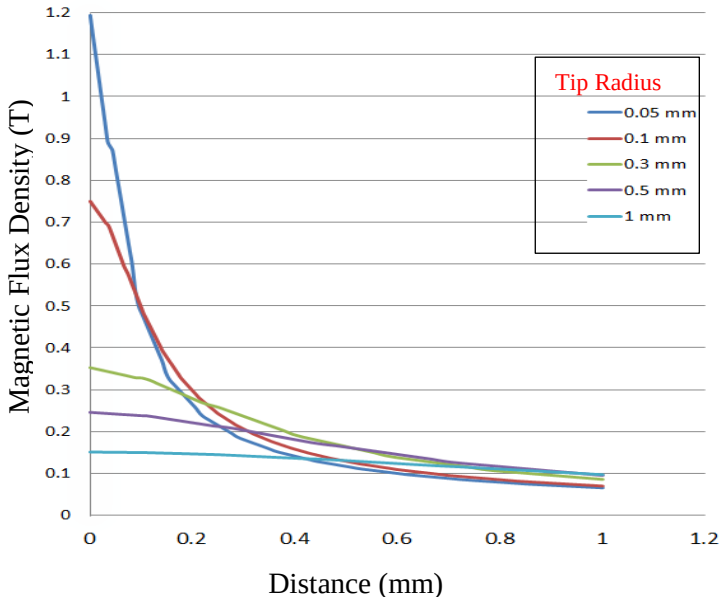

Figure 3.3.1.1 Magnetic flux density with different tip radii, the current in the coil is 0.5 A with 2000 turns, the core radius is 5 mm.

The change in tip radius from 0.05 mm to 1 mm will lead to a ten-fold increase in the magnetic flux density in the vicinity of the tip. Therefore our simulations show that the tip should be designed according to the position of a bead. While the tip radius is 1 mm the magnetic flux density is nearly 0.1 T for 1

mm away from the tip. The tip with 1 mm radius produces the effective magnetic flux density.

3.3.2 The effect of core radius

Figure 3.3.2.1 shows the magnetic flux density results inside the core and along 1 mm distance outside of the magnet for different radii. When the core radius is increased from 3 mm to 9 mm, the magnetic flux density decreases exponentially in the vicinity of the tip. But the magnetic flux density, 1 mm away from the tip diminishes fast. The highest magnetic flux density in the surface of the tip is obtained while the core radius was 3 mm. The field inside the magnet depends on the radius of the core as shown in Figure 3.3.2.1 (a). When the magnet core tripled, the flux density inside the magnet will show an approximately sevenfold increase. For a wider core, the flux density outside the magnet does not decrease exponentially, but for the narrower cores, magnetic flux density decreases exponentially. It can be said that the flux density inside the magnet greater than the outside of the magnet.

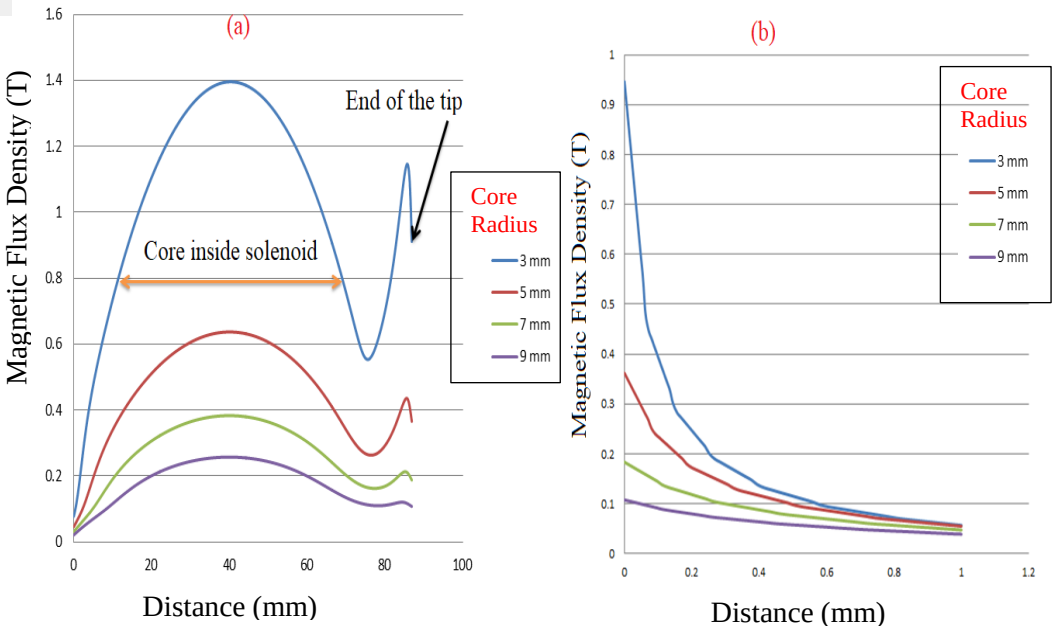

Figure 3.3.2.1 Magnetic flux density (a) inside the core and (b) along 1 mm outside the tip.

The simulations were done while the taper length equals to 13 mm and tip radius fixed at 1 mm.

3.3.3 The effect of taper length

Figure 3.3.3.1 shows the magnetic flux density for different taper lengths ranging from 4 mm to 20 mm. Since the magnetic force is a function of magnetic flux density, the changes in taper length have an impact on the force on a bead. The longer taper produces the highest magnetic force inside the magnet. But when we consider magnetic flux density outside the magnet, changes in taper length do not have too much impact on magnetic flux density near the tip. In this simulation the highest magnetic flux density is obtained while taper length is 13 mm. It should be regarded that taper length must be designed to meet optimum system configurations. Magnet with short taper length provides more linear relationship between distance and magnetic flux density. Therefore effective taper length design can be beneficial for electromagnet to produce more uniform magnetic forces.

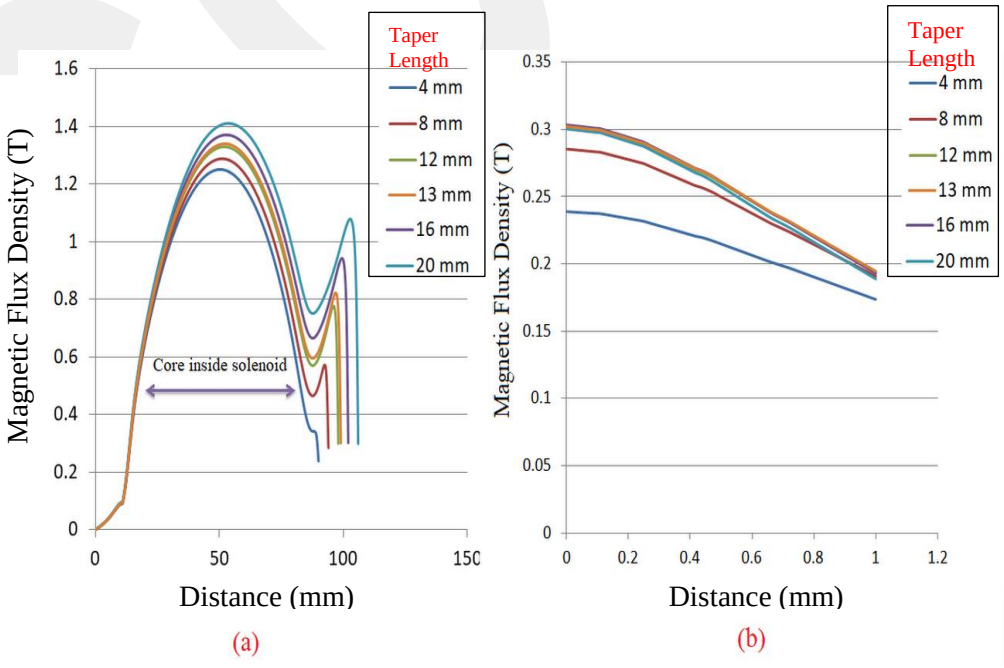

Figure 3.3.3.1 Magnetic flux density with different taper lengths (a) inside and (b) outside.

Simulation results reveal the fact that the magnetic flux density along 1 mm away from the magnet remains nearly the same but it has a significant effect on the surface of the tip.

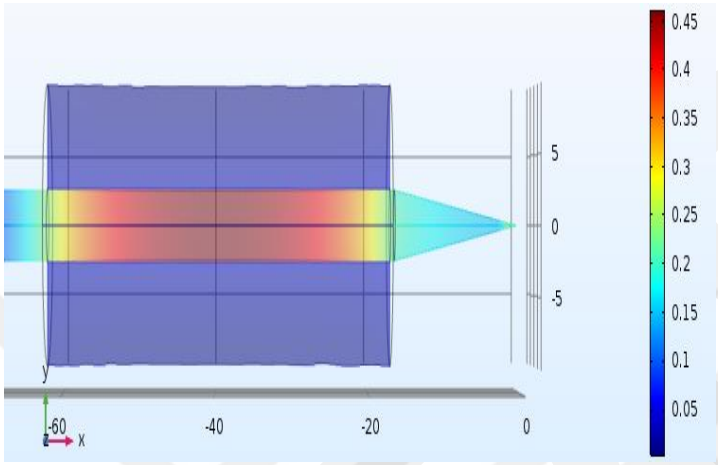

Figure 3.3.3.2 Magnetic flux density in the core.

Figure 3.3.3.3 shows that the flux density distribution on the surface of the tip.

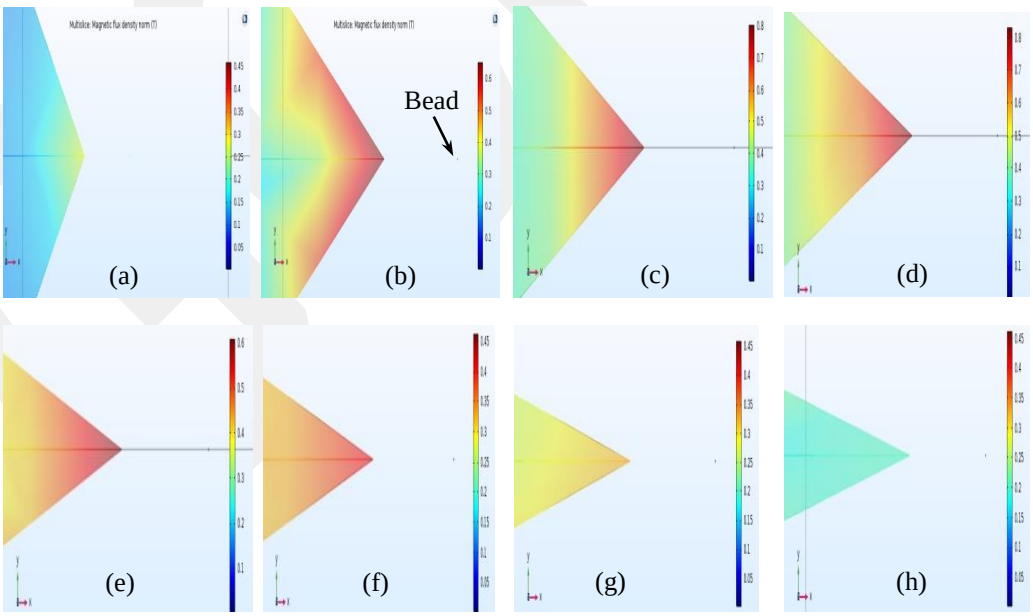

Figure 3.3.3.3 Magnetic flux density calculations for different taper lengths: a) 2mm, b) 4mm, c) 6mm, d) 8mm, e) 10mm, f) 12mm, g) 14mm, h) 16mm.

3.3.4 The effect of current

The changes in the current from 0.5 to 3.0 A are tested for magnetic flux density. It is clear from the figure 3.3.4.1 that current changes in the coil have a significant effect on the magnetic flux density generation. Figure 3.3.4.1 a, b shows the magnetic flux density level outside and inside the magnet respectively. Simulations show that magnetic flux density level both inside and outside the magnet increases with the increase in the coil current. However, this increase is not linear, as seen from the figure that the maximum flux differences h_1, h_2 and h_3 are not the same. Since the magnetic dipole moments inside the core begin to induce, every increase in current will lead to induces of the all magnetic dipole moments which accounts for saturation phenomenon. If we further increase the current level, all magnetic dipole moments will be induced by external magnetic field and magnitude of the magnetic flux density inside and outside the coil will not change due to the saturation of the core.

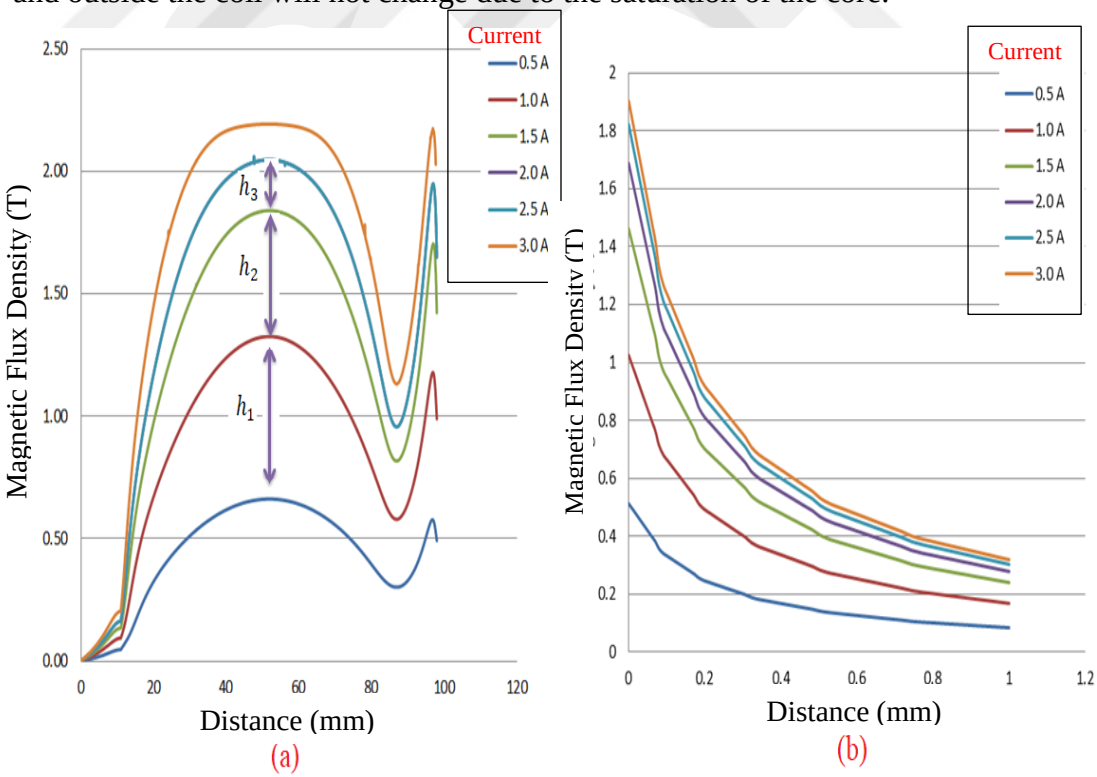

Figure 3.3.4.1 The current effect on magnetic flux density (a) inside and (b) outside the magnet.

In this simulation taper and core, lengths are fixed at 13 and 75 mm respectively, and the core and tip radius equal to 5 and 1 mm respectively. Lastly, flux density along 1 mm away from the magnet diminishes exponentially.

3.3.5 The effect of core length

The increment in the core length from 45 to 95 mm will result in an increase in the magnetic flux density both inside and outside the magnet. It seems that the changes in the core length have a significant effect on the magnetic flux density inside the magnet than in the proximity of the tip. When the core is excited by the external magnetic field, the magnetic dipole moments inside the core start to align in the direction of the magnetic field. Once all magnetic dipole moments get aligned, the increase in the magnetic field will not change the magnetic flux density due to saturation. Therefore magnetic core length must be appropriately adjusted for magnetic flux density during the high magnetic field. Saturation phenomenon should not be observed with a low magnetic field

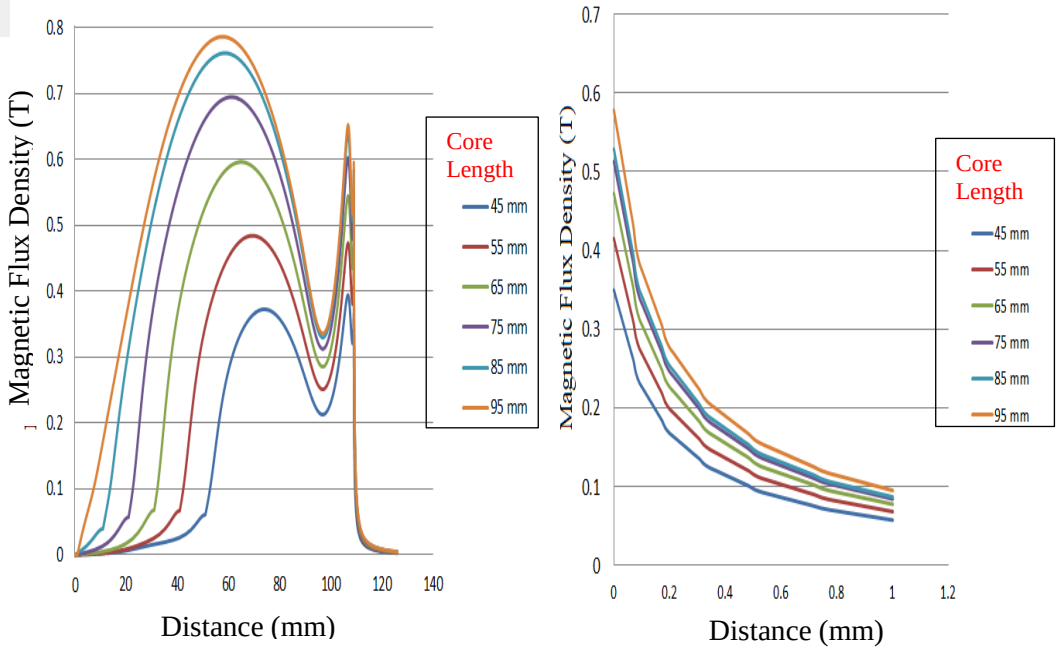

Figure 3.3.5.1 Flux density distribution with various core lengths.

3.3.6 The effect of solenoid position

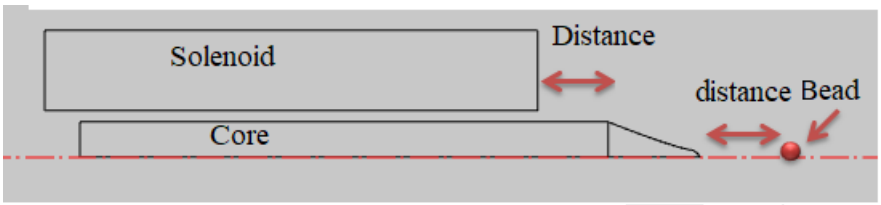

Figure 3.3.6.1 Schematic representation of a single solenoid.

Magnetic flux density simulation results are carried out according to this representation

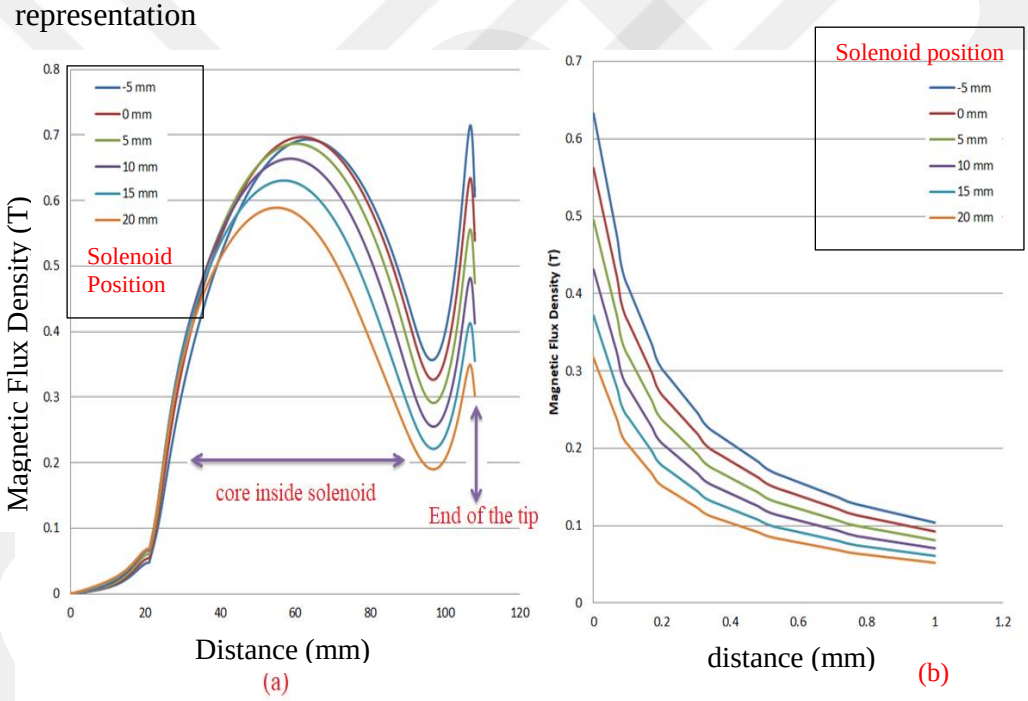

Figure 3.3.6.2 Magnetic flux density distribution (a) outside and (b) inside the magnet with different solenoid position.

Here, we investigated that how the position of the solenoid effect magnetic flux density inside and outside the magnet. It can be observed from the Figure 3.3.6.1 that, the maximum flux density can be obtained in the vicinity of the solenoid tip. Therefore the solenoid should be placed close to the tip in order to produce higher magnetic flux density.

3.3.7 The comparison of experimental and numerical results

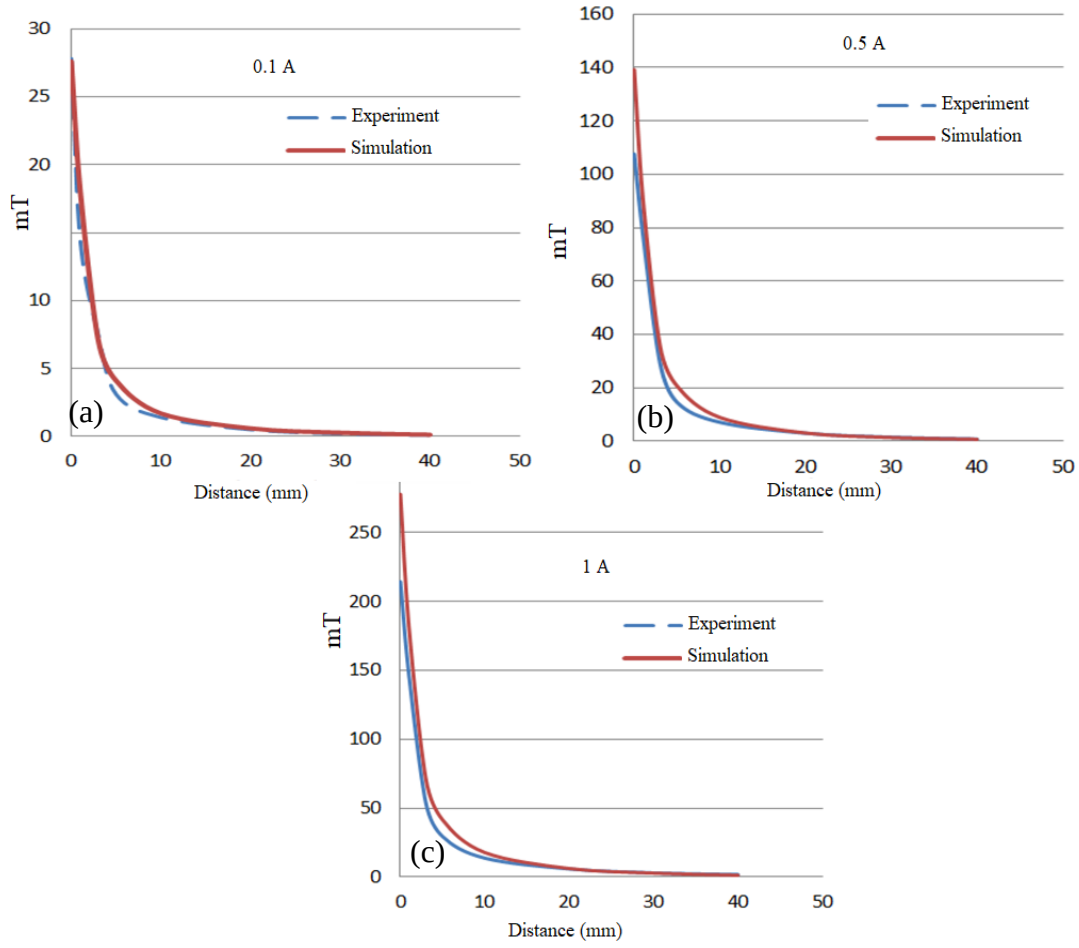

Figure 3.3.7.1 Comparison results between experiment and simulation.

A single needle tip (Figure 3.3.6.1) was tested in order to compare simulation and experimental results. Figure 3.3.7.1 shows that magnetic field changes versus distance along the tip. The magnetic field was measured in every 5 mm gap with Gauss Meter. These results were combined and illustrated in figure (a), (b) and (c). Magnetic field changes, in the simulation with low current, are almost the same with experimental results. While current is increased, the magnetic field near the tip is greater than experimental results but it follows the same path and diminishes exponentially.

3.4 Multi-pole Magnetic Tweezers

In this section, various magnetic tweezers concepts are addressed for optimum designs and two-pole or horizontal magnetic tweezers and quadrupole magnetic tweezers were designed and analyzed in Comsol Multiphysics.

3.4.1 Horizontal Magnetic Tweezers

Firstly two-pole magnetic tweezers are designed in order to understand magnetic flux density effects on each other. The distance between two tips is set 8 mm and low carbon steel is chosen for magnetic flux density analysis. This horizontal system can apply one dimensional force on a bead. For effective particle manipulation, horizontal magnetic tweezer should produce uniform flux distribution in order to control a particle accurately.

Surface: Magnetic Flux Density Norm (T), Arrow Surface: Magnetic Field

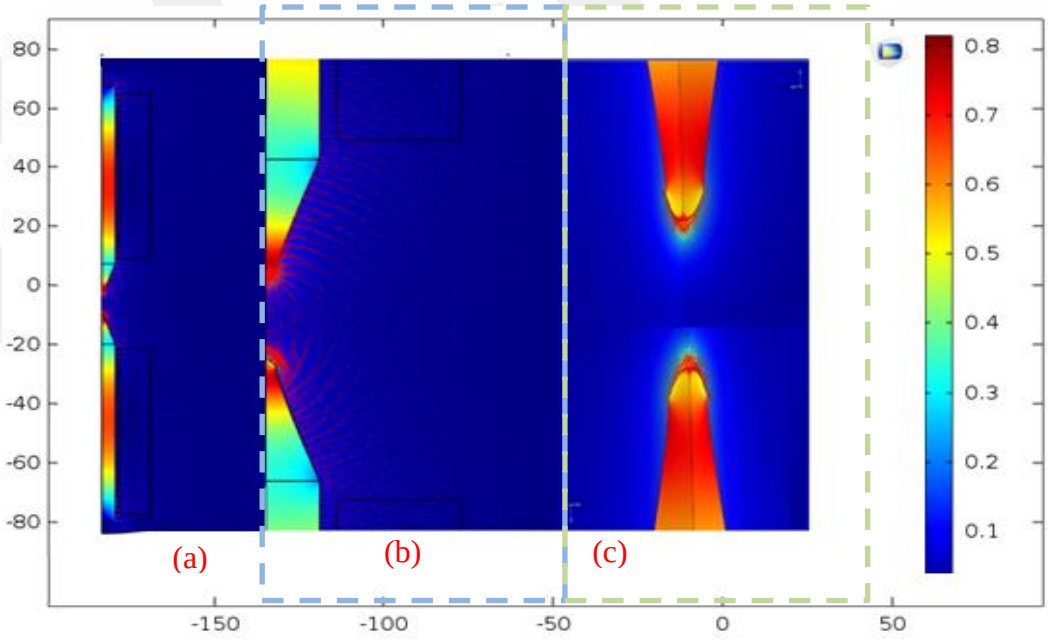

Figure 3.4.1.1 Magnetic flux density norm in the core material (b) and (c) show a closer look at the apex of the tip.

3.4.2 Quadrupole Magnetic Tweezers

Quadrupole magnetic tweezers can be used in two dimensional position control of superparamagnetic bead via external magnetic field generation. Hence a four-coil based configuration is considered for symmetric force generations.

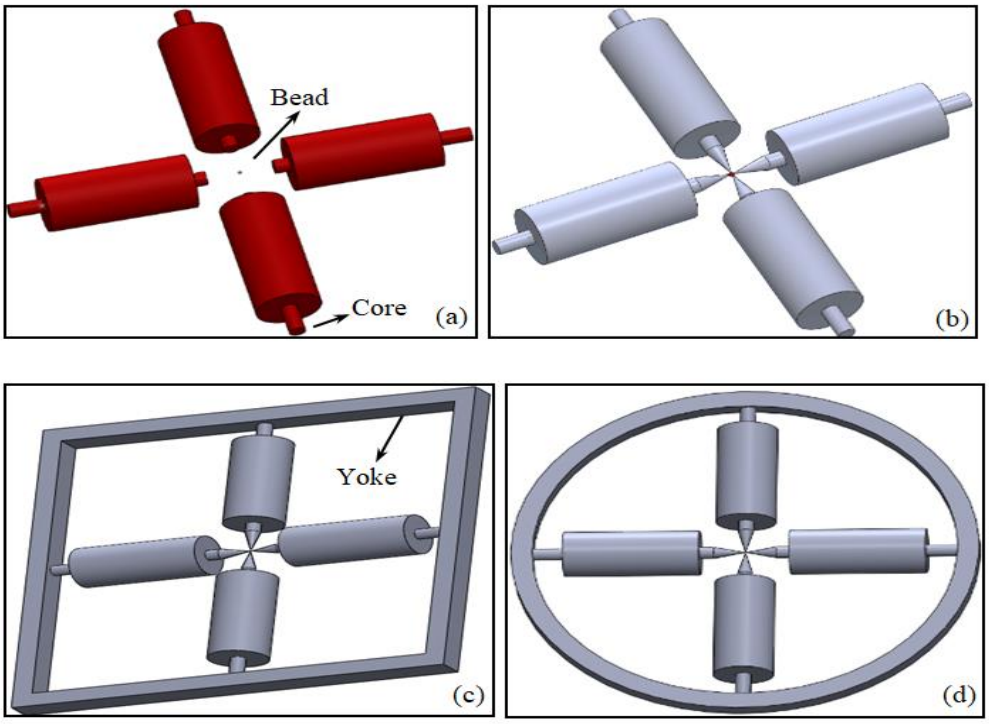

Figure 3.4.2.1 Different magnetic actuator design concepts.

Figure 3.4.2.1 shows various CAD designs. It is found that while the first design is given in Figure 3.4.2.1-a produces the weakest magnetic flux density on the tip of the core, the designs illustrated in Figures 3.4.2.1 c and d produces the strongest magnetic flux density on the sharp tips. Designs with yokes generate higher magnetic density than designs without yoke since the yoke creates a path for magnetic field circulation. Another important point is that the shape of the yoke does not have a noticeable impact on magnetic flux density whether circular or square. All these results are obtained from the Comsol simulations.

Chapter 4

Modeling and Control

4.1 Magnetic Force Modelling

When a superparamagnetic bead is exposed by a non-uniform magnetic field, the magnetic field gradient will induce a magnetic moment of the particle and then induced magnetic moment will form a potential given by $U = -m \times B$ [26]. The magnetic force on a bead is a conclusion of given equation and can be obtained from the following equation [27].

$$F = 0.5\nabla(m(B).B) \quad \textbf{(4.1.1)}$$

where m(B) is the magnetic moment of the particle and B is the magnetic flux density. It is clear that the magnetic force exerted on a bead is proportional to the magnetic moment of the bead and magnetic flux density. For large external magnetic field, by considering saturation condition the force can be defined by

$$F = 0.5\nabla(m_{sat}.B) \quad \textbf{(4.1.2)}$$

Magnetic moment of the particle can be obtained by

$$m = V_m M \quad \textbf{(4.1.3)}$$

By substituting **(2.3.3)** into the **(2.3.1)** and H is given and the final form of magnetic force can be calculated by

$$F = V_b \chi \nabla |B|^2 / 2\mu_0 \quad \textbf{(4.1.4)}$$

4.1.1 Dynamics of Magnetic Particles

When a magnetic bead has a movement in a fluid environment, the magnetic bead will be experienced by drug force or Stokes force due to the viscosity of the liquid. According to Newton's second law of motion, particle dynamics can be obtained as

$$m\ddot{x} + \sigma\dot{x} = F_m + F_t + F_g + F_o \quad \textbf{(4.1.1.1)}$$

where m is the mass of the particle, σ is the drag coefficient of the bead in water. In addition to magnetic (F_m) and hydrodynamic drag force $(F_d = \sigma\dot{x})$, there have been a thermal force (F_t) known as Brownian motion, gravity force (F_g) and other forces (F_o) experienced by a bead. The Stokes drug force exerted on a moving bead can be calculated by

$$F_d = \sigma\dot{x} = 6\pi\eta\beta Rv \quad \textbf{(4.1.1.2)}$$

where η is the dynamic viscosity of fluid and R is the radius of the bead and v is the velocity of the bead and σ is the drag coefficient for a spherical particle in a viscous fluid and can be calculated [29].

$$\sigma = 6\pi\eta\beta R \quad \textbf{(4.1.1.3)}$$

where β is the correction factor varying as $1 \leq \beta \leq 3$. Thermal force results from the random movement of particles that are caused by collisions in the fluid with smaller particles such as liquid or gas molecules. Thermal force can be calculated as [30-31],

$$F_t = \delta(2\sigma k_B\, T/T_S)^{0.5} \quad \textbf{(4.1.1.4)}$$

where δ is the white noise with zero mean and unit variance, T_S is the sampling time, and k_B is the Boltzmann constant.

The thermal force is described with a white noise whose power spectrum density is obtained

$$PSD(F_t) = 4k_BT\sigma \quad \textbf{(4.1.1.5)}$$

The gravitational force is given by [31] and results from gravity and buoyancy

$$F_g = -V_p(\rho_p - \rho_f)g \quad \textbf{(4.1.1.6)}$$

where V_p, ρ_p, ρ_f and g are volume of the particle, the particle density, fluid density, and the acceleration of gravity, respectively.

4.1.2 Demagnetization field

Once a magnetic material is magnetized by an external magnetic field, it creates an internal magnetic field which points opposite to the magnetization that is called demagnetization.

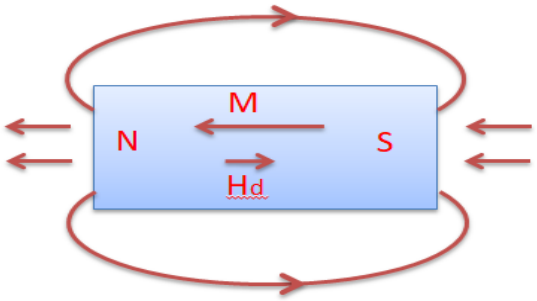

Figure 4.1.2.1 Demagnetization factor for a magnet.

Demagnetization effect depends on the geometry of a material. For spherical materials demagnetization factor can be calculated by [32]

$$H_d = \frac{-1}{3} M \qquad \textbf{(4.1.2.1)}$$

The total magnetic field inside the spherical material is given by

$$H_{in} = H_e + H_d \qquad \textbf{(4.1.2.2)}$$

where H_e is the external magnetic field, and total magnetic field can be calculated by substituting **(4.1.2.1)** into equation **(4.1.2.2)**

$$H_{in} = H_e - \frac{1}{3} M \qquad \textbf{(4.1.2.3)}$$

equation **(2.1.2)** is used to calculate magnetization inside the sphere

$$M = \frac{3(\mu - \mu_o)}{\mu + \mu_0} H_e \qquad \textbf{(4.1.2.4)}$$

Since the magnetic moment depends on the volume of the particle, it can be obtained by equation **(2.1.3)** and **(2.1.1)**

$$m = \frac{3V_b}{\mu_0} \frac{(\mu - \mu_0)}{(\mu + 2\mu_0)} B \qquad \textbf{(4.1.2.5)}$$

Magnetic moment of the particle is calculated for the spherical object hence the force is written as

$$F_m = \frac{3V_b}{\mu_0} \frac{(\mu-\mu_0)}{(\mu+2\mu_0)} (B.\nabla)B \qquad \textbf{(4.1.2.6)}$$

To find the magnetic force, the components of the magnetic field vector are needed to be known. In order to calculate magnetic force acting on a bead, the empirical results and point magnetic charge approach can be used to simplify the force calculations. The magnetization or magnetic moment of the magnetic particles have been determined experimentally in some studies. The tip of pole is assumed as a point magnetic pole to calculate the magnetic force, the generated magnetic field at a position r by the magnetic charge q can be given by [33].

$$B = k_m \frac{q}{r^2} \hat{u} \qquad \textbf{(4.1.2.7)}$$

where $r(in\ m)$ is the vector result from the location of the magnetic charge to the magnetic particle, q (in Am) is the magnetic charge, $\hat{u}$ is the unit directional vector, and $k_m = \mu_0/4\pi$ .Therefore the produced force can be written as

$$F_m = \frac{4k_Q {k_m}^2}{d^5} q^2 \hat{u} \qquad \textbf{(4.1.2.8)}$$

where, $k_Q = 3V_b(\mu - \mu_0)/(2\mu_0(\mu + 2\mu_0))$ and $r = d$(in m) is the radius of workspace. The relation between magnetic charge, ϕ and magnetic flux, μ_0 can be defined as

$$q = \phi/\mu_0 \qquad \textbf{(4.1.2.9)}$$

We consider that whole magnets are identical hence the implementation of the Ampere's loop law to magnetic circuit results in

$$\phi = N_c I/R_a \qquad \textbf{(4.1.2.10)}$$

where $N_c$is the number of turns of the coils, R_a is the magnetic reluctance of the air gap, given by $R_a = g_a/(\mu_0 A_a)$, g_a (in m) is the air gap and A_a (in m^2) is the cross-section area. The magnetic force model for horizontal electromagnets at the center of the workspace ($x=0$) is obtained as [33]

$$F_m = \left(\frac{k_Q k_m^2}{d^5} \right) \left(\frac{2N_c}{\mu_0 R_a} \right)^2 \left(I_1^2 - I_2^2 \right) \qquad \textbf{(4.1.2.11)}$$

Equation (4.1.2.11) represents the magnetic force to the current relation of the horizontal tweezer around the workspace center. We neglect other forces since the electromagnets produce relatively high magnetic force. It is clear that magnetic force and drug force are the most effective forces compared to lift force, particle-particle interaction force, magnetic interaction force, van der Waals attraction force, thermophoretic force, and electrostatic interaction force. Specifically the magnetic force must be sufficiently produced to meet the desired control actions.

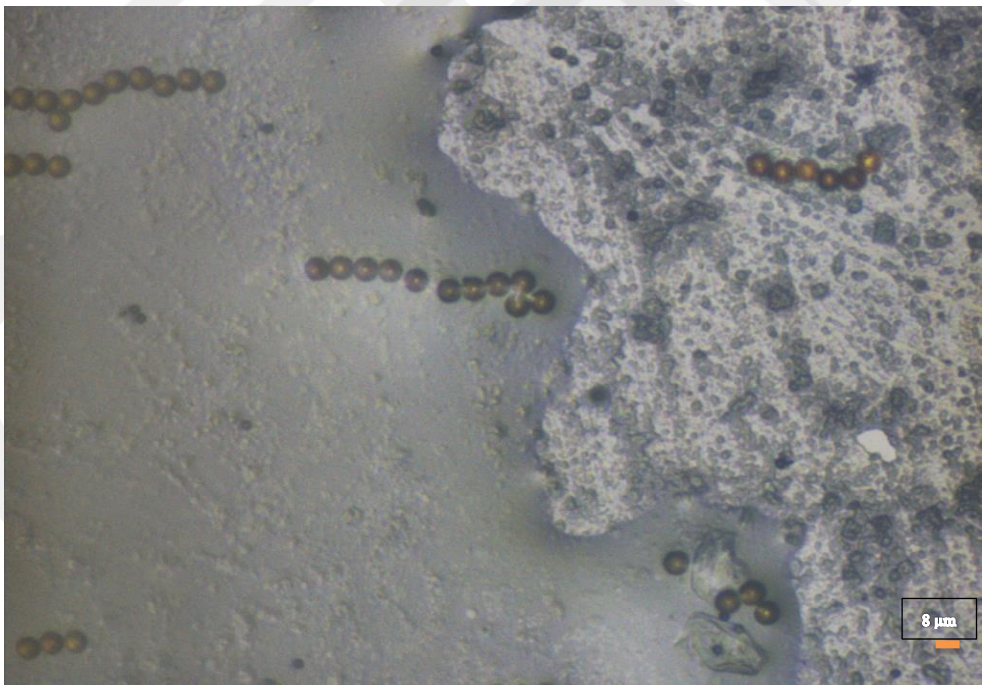

Figure 4.1.2.2 Agglomeration of 8 µm magnetic particles under an external magnetic field.

4.1.3 Control Design

In this study, one dimensional and two dimensional controllers are tested. The linear controller is designed to control the magnetic microparticles. An offset current with the magnitude of I_0 is used in the controller design given by [34],

$$I_1 = 0.5(I_0 + K_p(x_{ref} - x)) \quad \textbf{(4.1.3.1)}$$

$$I_2 = 0.5(I_0 - K_p(x_{ref} - x)) \quad \textbf{(4.1.3.2)}$$

where K_p is a control gain, x_{ref} is a constant position reference, and x is the measured position. The tracking algorithm is achieved using two and four magnetic poles with image processing based feedback controller. The single superparmagnetic particle with 8 µm is chosen for the experiment.

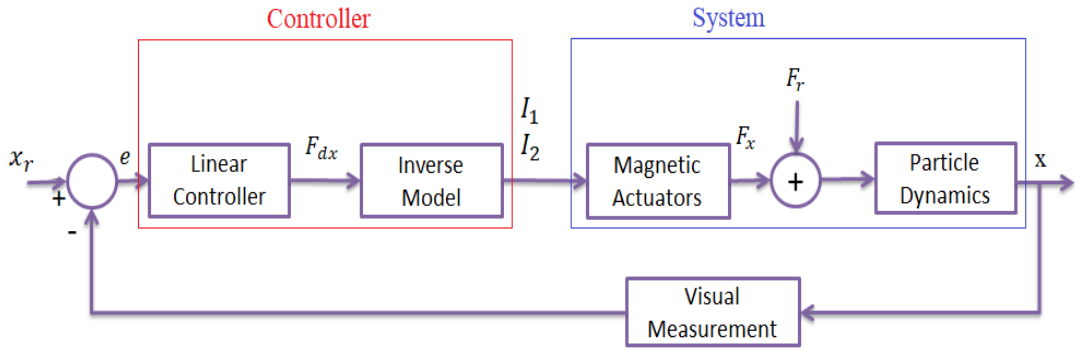

Figure 4.1.3.1 Control diagram for horizontal magnetic system.

4.2 One Dimensional Position Reference

In this section, one dimensional position reference signals were considered, the controller is applied, and tracking performance of the particles are observed.

4.2.1 Bump Position Reference

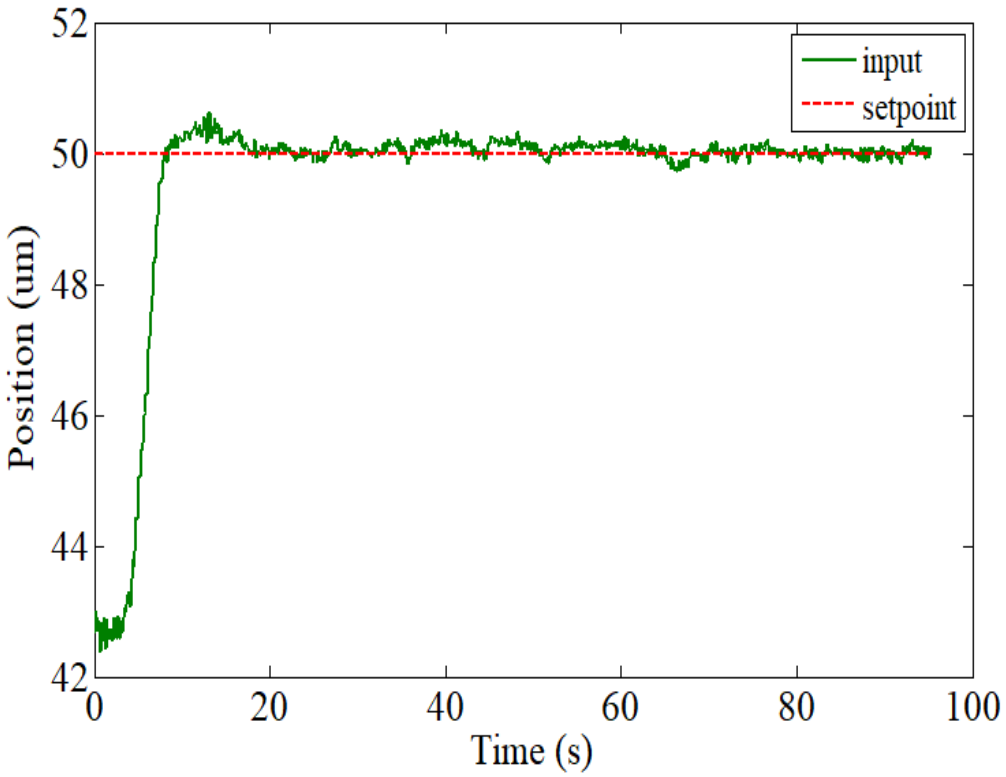

Figure 4.2.1.1 Experimental particle position trajectory in the x-axis.

Figure 4.2.1.1 shows that the particle tracking reference trajectory from 43 um to 50 um and the electromagnetic system holds the particle in a given setpoint. P controller is used to controlling the position of the particle with the desired location which equals 50 um and the K_p value is chosen 0.8×10^{-6} to

satisfy the desired position. It is shown in Figure 4.2.1.2 represents position error of the particle which results from thermal noise and measurement error.

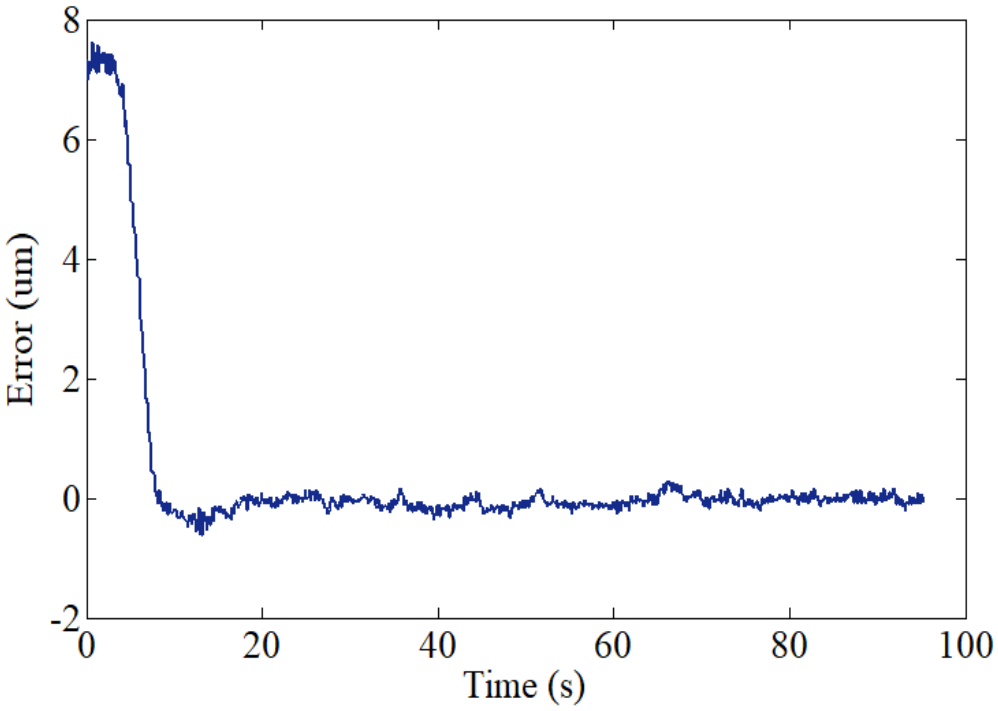

Figure 4.2.1.2 Experimental particle position trajectory error in the x-axis.

Figure 4.2.1.3 shows coil currents which are utilized to balance the bead in the desired position for 95 seconds. The I_1 and represent I_2 coil currents. In order to steer the magnetic particle to the desired position without any magnetic saturation, the maximum coil current was limited to 1 A. It is clear from the figure that the experimental results are highly satisfactory with a zero-steady error. The steady-state control currents are 0.5 A.

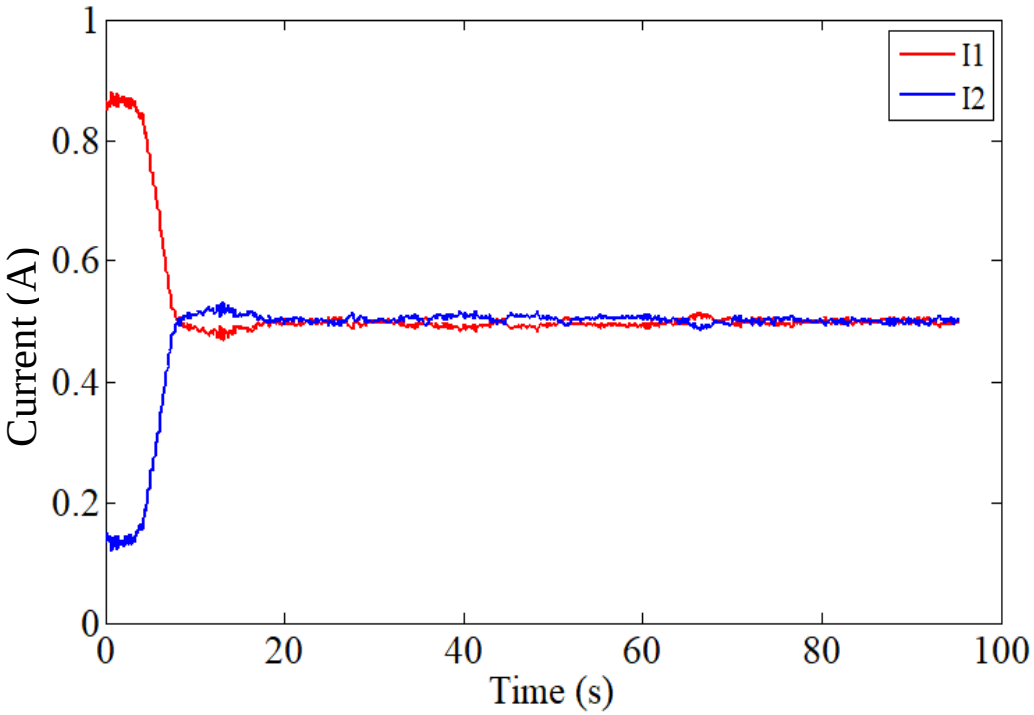

Figure 4.2.1.3 Experimental coil currents for one dimensional system.

Figure 4.2.2.1 shows the particle position trajectory with the sinusoidal reference signal. The input represents bead position and the setpoint represents reference sinusoidal signal. The first location of the particle was 40 µm. Therefore the position error is the maximum.

When the magnetic system is run, the particle moves the reference point in order to catch the reference signal. Magnetic particle reached the reference point within 7 seconds. Figure 4.1.2.2 shows the position error of the particle. It is seen that the position error reaches around zero and show some fluctuations due to the thermal noise and measurement error.

4.2.2 Sinusoidal Reference

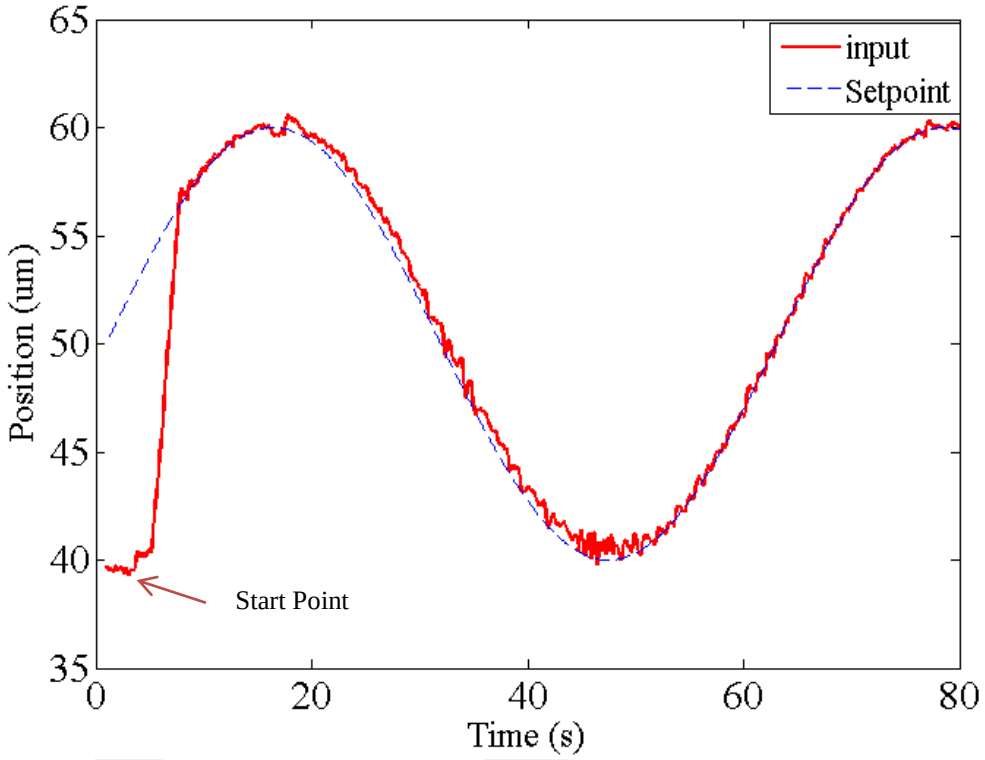

Figure 4.2.2.1 Experimental particle position trajectory for sinus reference signal.

The coil current response is illustrated in Figure 4.2.2.3, the magnetic system starts with maximum coil current due to the first position of the particle and reaches around 0.5 A.

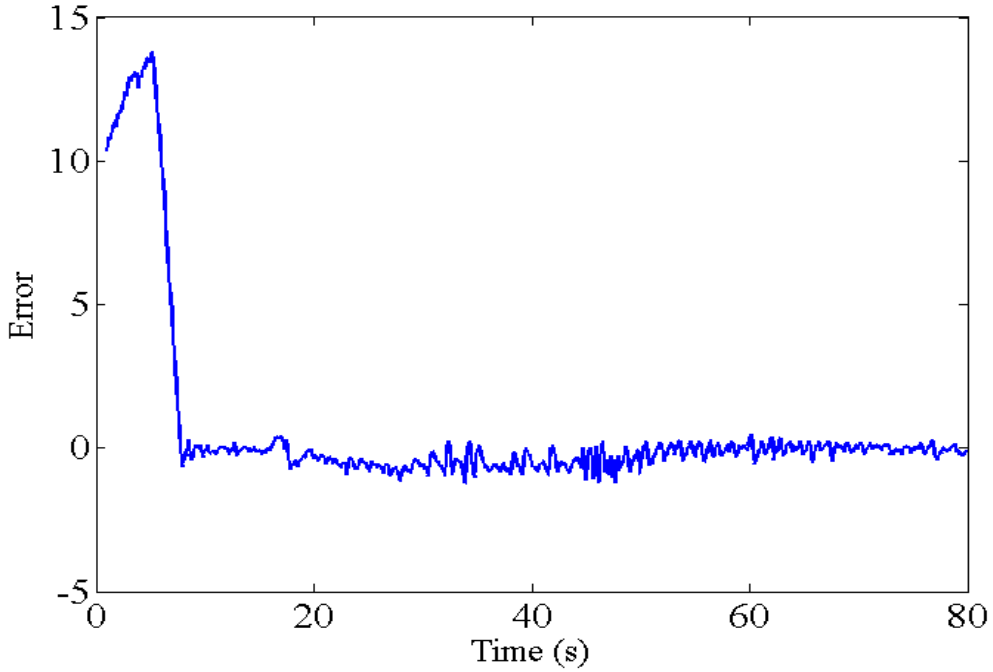

Figure 4.2.2.2 Experimental particle position error for horizontal magnetic system.

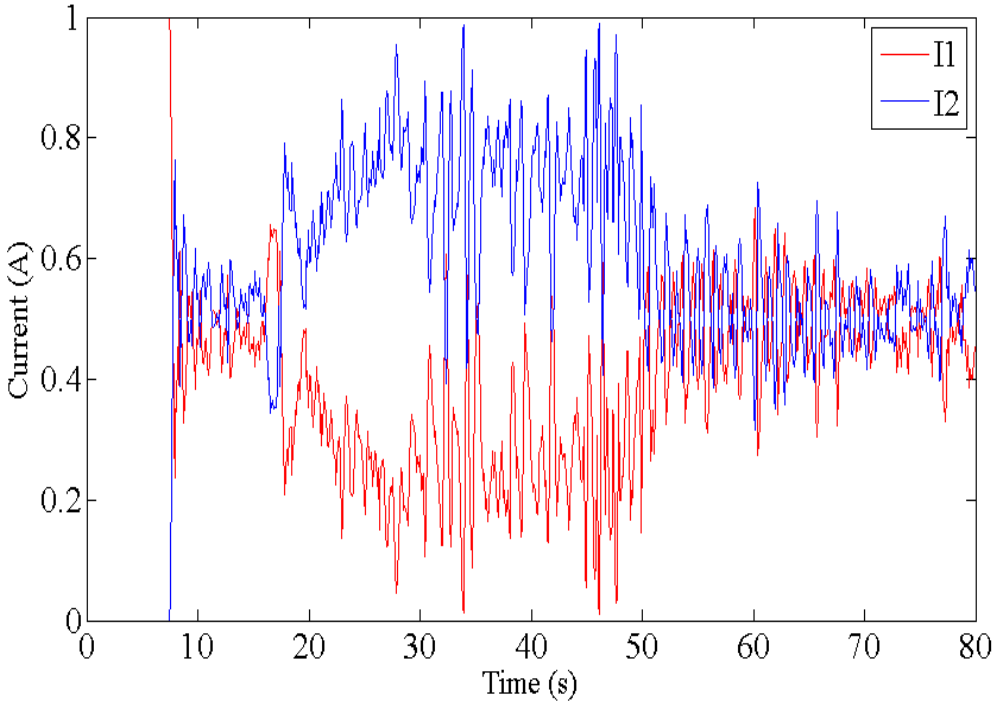

Figure 4.2.2.3 Experimental coil currents response for horizontal magnetic system.

4.2.3 Square Wave Reference

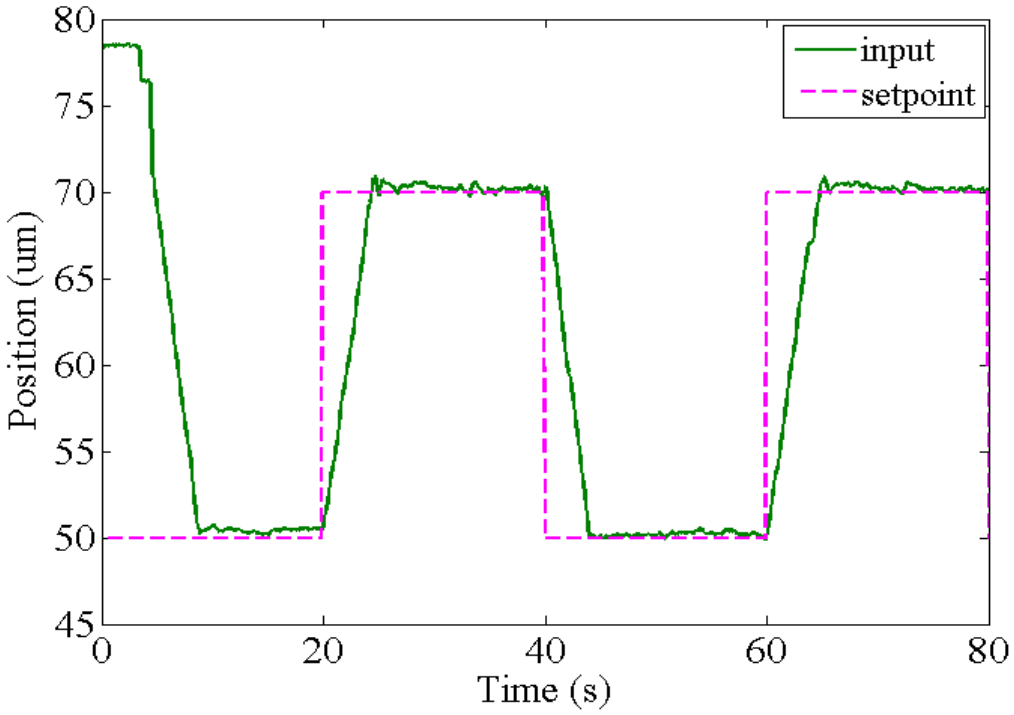

Figure 4.2.3.1 Experimental particle position trajectory for square wave signal.

Figure 4.1.3.1 shows the position of the particle with the square reference signal. When the reference signal is applied, the bead position was 77 µm in the x-axis and then the particle begins to track the reference signal by reducing position error which is illustrated in Figure 4.2.3.2**.** In the beginning of the system, the maximum error was 30 µm due to the first position of the particle thereafter the position error reaches around zero. The coil currents are illustrated in Figure 4.2.3.3.

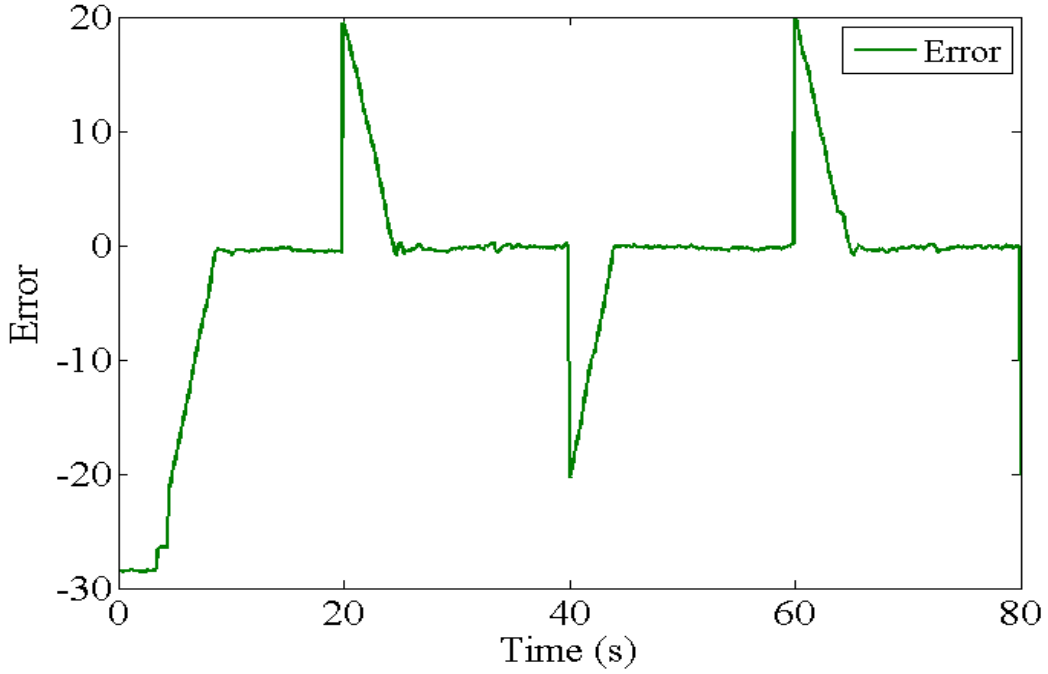

Figure 4.2.3.2 Experimental particle position error for the horizontal magnetic system.

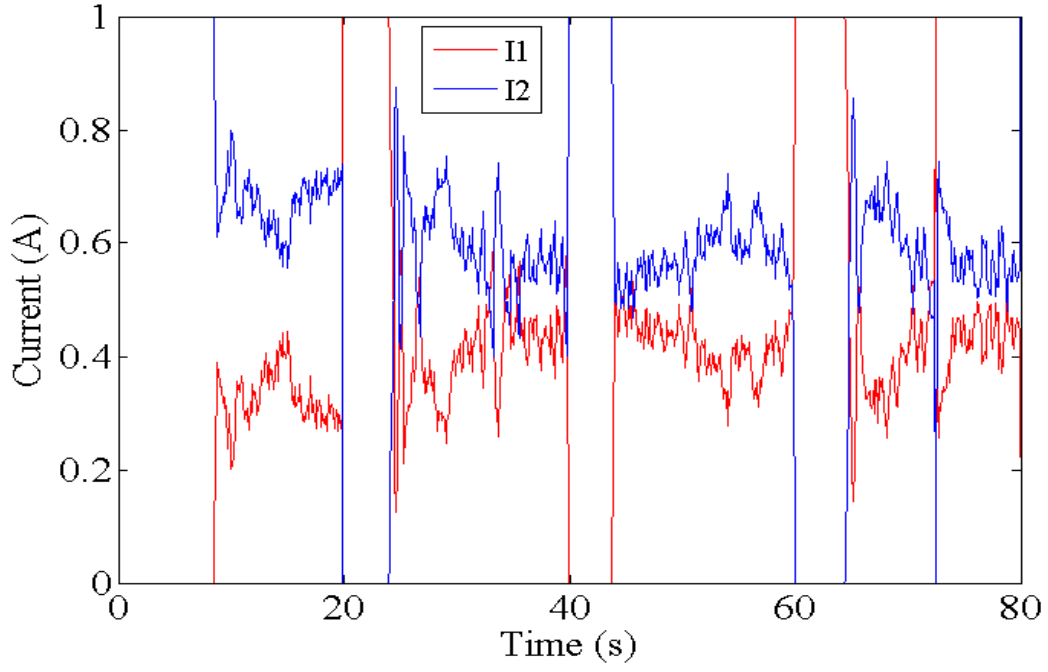

Figure 4.2.3.3 Experimental coil currents response for the horizontal magnetic system.

4.3 Extention to Two Dimensional Control

In this section, we added new magnetic poles in order to enhance the maneuverability of the particle. This feature brings new problems such as vibration of coils and position calibration. Since the magnetic system consists of 2000 copper turn, it produces a highly strong magnetic force which causes magnets to pull towards each other. The changes of pole position lead to an unbalanced magnetic force on a bead that results in low position tracking performance. Another problem that we encounter is that the position calibration of the particle is difficult to be adjusted correctly. The magnetic particle should be placed to the middle of the working center because magnetic particle deviates from the reference path due to the unequal distance between each of magnetic tips and the particle. We solved this problem by the recording of particle positions in the motorized manipulator.

4.3.1 Square Reference

Figure 4.3.1.1 shows the position of the particle with a square reference path. The green lines represent the path which is taken by the particle and the dashed lines represent reference path. The first position of the particle is illustrated in Figure 4.3.1.1. And it tracks reference path for 120 seconds. The controller was set to holds the particle with a limited time in the corners. The position error which is illustrated in Figure 4.3.1.2 is around the 1.8 µm due to thermal noise and magnetic interactions. Figure 4.3.1.3 shows the coil current changes for the square path. I_1 and I_2 are the current sources for x axes. I_3 and I_4 are the current sources for y axes.

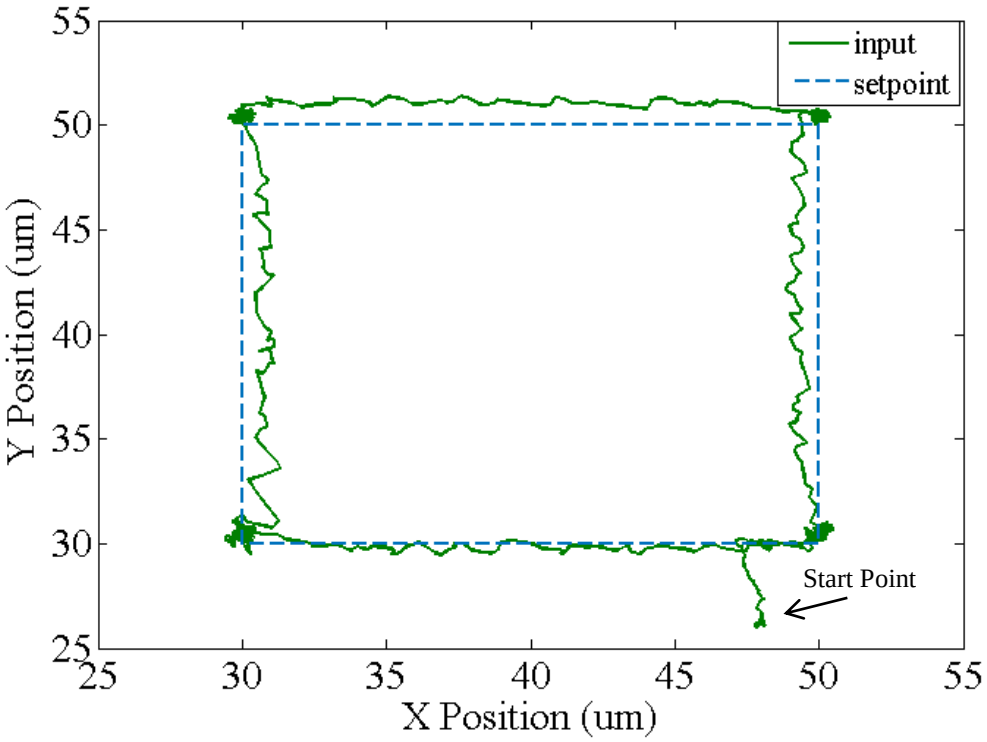

Figure 4.3.1.1 Experimental tracking performance of a square trajectory.

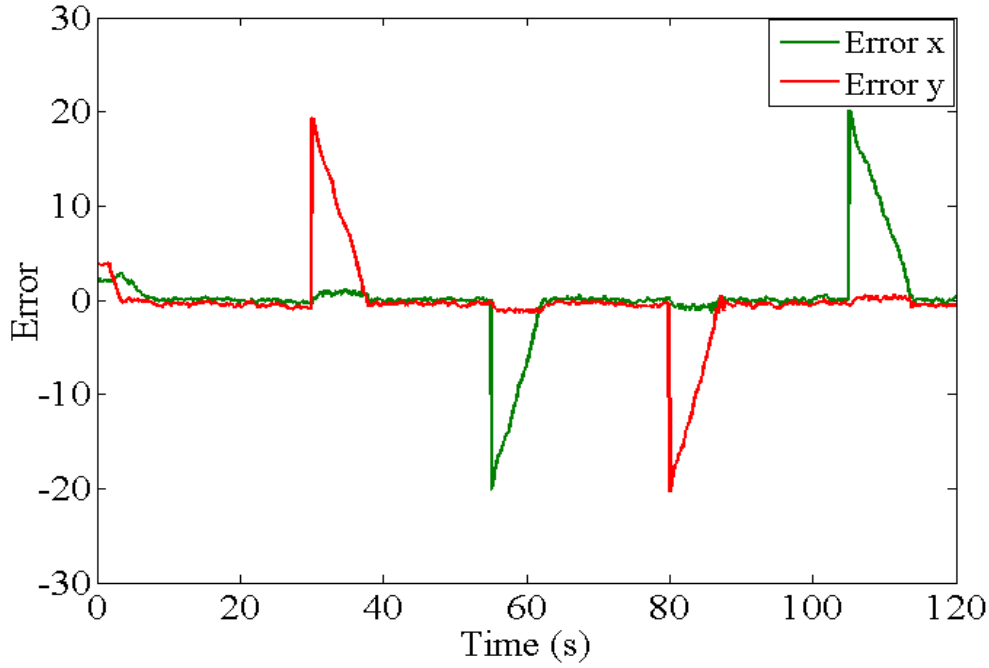

Figure 4.3.1.2 Position error of the particle in x and y-axis.

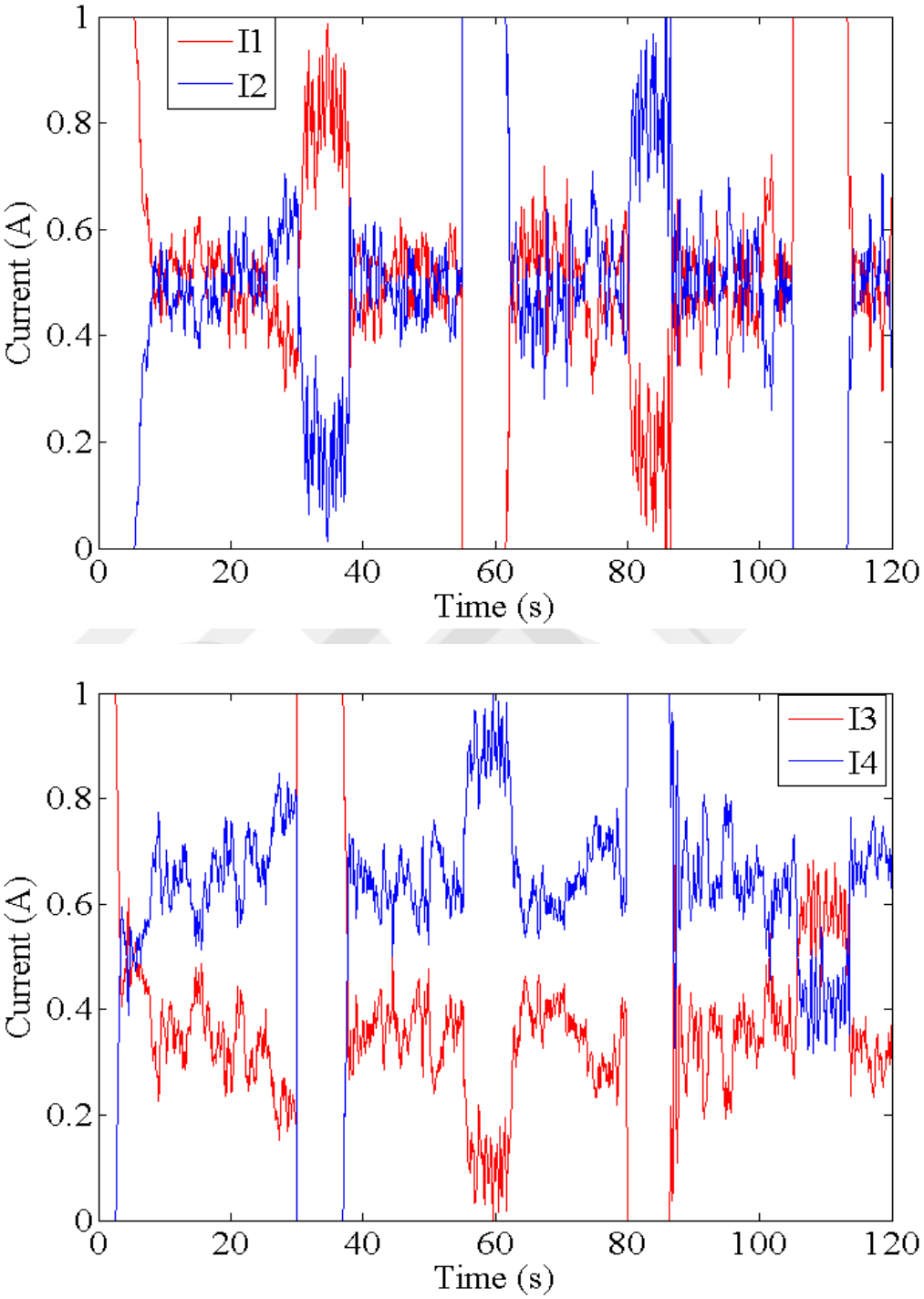

Figure 4.3.1.3 Coil currents for the square path.

4.4 Transportation of B Type Leukemia Cell

To demonstrate one of the biomedical applications of the micro manipulator system, the immunomagnetic beads 4.5 µm superparamagnetic particles coated with CD19 antibody [35] are used to bind to B type leukemia cells. After incubation of immunomagnetic particles and leukemia cells, captured cells are placed in the fluidic reservoir. Figure 4.4.1-a shows schematic representation of cell and beads.

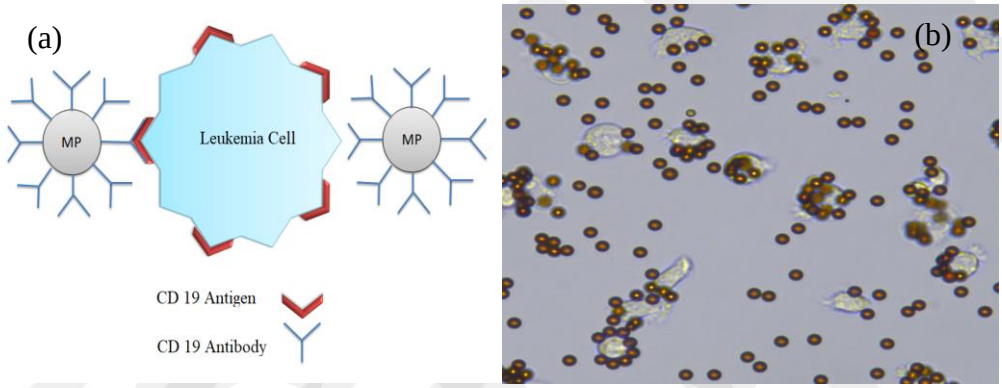

Figure 4.4.1 Schematic representation of magnetic beads with leukemia cell (a), the images (b) of leukemia cell conjugated with magnetic particles taken by Nikon microscope.

Transportation of leukemia cell is achieved by applying an external magnetic field, which is created by the designed electromagnets. Figure 4.4.2 shows the movement of the particle from initial position (x=-32 µm, y=20 µm) to final position (x=-240 µm, y=245 µm). The average velocity of the particle is calculated around the 3.64 $\mu m/s$. The video link is available in Youtube: https://www.youtube.com/watch?v=sNu8GaH2Rlg

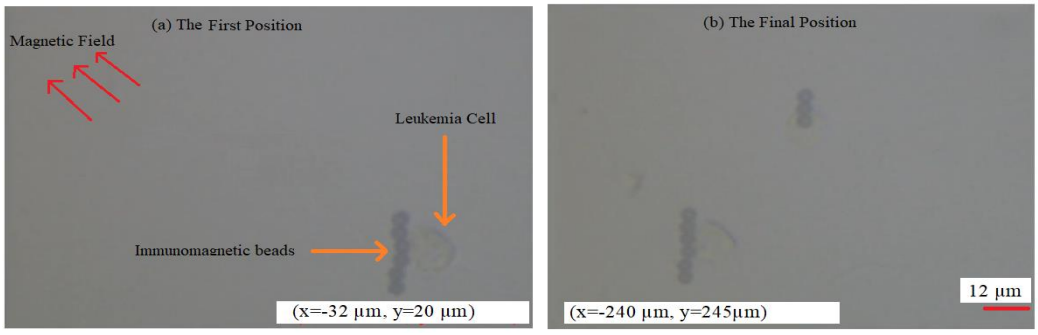

Figure 4.4.2 Transportation of Leukemia cell by using external magnetic field (a) initial position, (b) Final position.

Chapter 5

Conclusion and Future Prospects

5.1 Conclusions

For one and two dimensional manipulations, various magnetic tweezers concepts were designed and analyzed for optimum flux generation. In this study, the powerful numerical solvers are used to quantitatively predict the magnetic forces, and systematically investigate the effects of different electromagnet geometries and configurations. Also, we compared numerical and experimental solutions. The behavior of soft magnetic material was observed under the high magnetic field. Since magnetic force is the square gradient of the magnetic field, the force acting on a bead can be predicted via numerical solutions.

The simulation results indicate that the highest magnetic flux density was observed in the vicinity of the tip. The force acting on a bead diminishes exponentially along the core axis. Therefore a particle should be placed near the tip in order to obtain high pulling forces. Comsol Multiphysics was used to understand the magnetic flux density distributions on the surface of the tip and inside the core with different geometries. These results can be listed as follows, when the core radius is increased the flux density in the vicinity of tip would decrease, when the tip radius is decreased, this will lead to an increase of magnetic flux density. When the taper length is increased, this will lead to an increase of magnetic flux density in the core. When the length of the core is decreased, this will lead to a decrease in magnetic flux density. Higher current in

the solenoid produces higher magnetic flux density in the vicinity of the tip. An electromagnet with yoke produces higher magnetic flux density than electromagnet without the yoke [37].

In this research, a linearizing feedback controller is used to control magnetic particles in the desired region. Two dimensional control and manipulation is achieved with P control. The magnetic system capable of controlling magnetic particles with a 2x2 mm reservoir due to the optimum geometry of the core and tip. It is highly satisfactory because of low-cost production. Less than 1 A current input, up to 25 pN force is generated on the particles. Quadrupole magnetic tweezers can be used in cell manipulation, drug delivery, and hyperthermia. Therefore it has a crucial role in biomedical and electronics. In order to obtain high tracking performance K_p constant around $0.8\text{x}10^{-6}$ is adjusted in the experiment. To increase image resolution, the background of the reservoir is chosen dark. In order to avoid saturation phenomenon, the coil currents are limited to less than 1 A.

The results of this study are compared with the previous works in the literature in Table 5.1. While a direct comparison is not possible because almost all designs have different features in terms of material, geometry, configuration and workspace size.

Performance	This work	Previous works	
Coil current (Max)	1 A	3 A	[36]
		4 A	[37]
		0.9 A	[38]
		0.028 A	[39]
		3 A	[40]
Speed of Control loop	10 Hz	<40 Hz	[36]
		303 Hz	[37]
		200 Hz	[38]
		10 Hz	[39]
		<25 Hz	[40]
Position error	<0.25 µm	40nm	[36]
		0.1-0.7 µm	[37]
		0.15 µm	[38]
		~2 nm	[39]
		Not available	[40]
Pole Number	4-2	1	[36]
		6-3	[37]
		6-4	[38]
		6	[39]
		3-4	[40]
Force	~25 pN	<100 nN	[36]
		<400pN	[37]
		Few pN	[38]
		<20pN	[39]
		1-120 pN	[40]
Workspace size	2 x 2 mm^2	100 µm	[36]
		0.1 x 0.1 mm^2	[37]
		405 x 405μm^2	[38]
		2 x 2 mm^2	[39]
		20 x 20 μm^2	[40]
Maneuverability	1D feedback control	1D force control	[36]
	2D feedback control	2D feedback control	[37]
		2D feedback control	[38]
		3D feedback control	[39]
		2D non-feedback control	[40]

Table 5.1 Comparison of magnetic tweezers

5.2 Future Prospects

We will conjugate different types of biomolecules on the surface of the beads to steer desired points. We will develop a tiny magnetic system which will be capable of three dimensional control and manipulations. The new magnetic micromanipulation system will be more portable and fully automatic. We will try to increase the sampling frequency by implementing some new image-based algorithms.

BIBLIOGRAPHY

[1] J. Yan, D. Skoko, and J. F. Marko, "Near-field-magnetic-tweezer manipulation of single DNA molecules," *Phys. Rev. E*, vol. 70, no. 1, p. 011905, Jul. 2004.

[2] L. Sacconi, "Three-dimensional magneto-optic trap for micro-object manipulation," *Opt. Lett., OL*, vol. 26, no. 17, pp. 1359–1361, Sep. 2001.

[3] E. J. G. Peterman, F. Gittes, and C. F. Schmidt, "Laser-induced heating in optical traps," *Biophys. J.*, vol. 84, no. 2 Pt 1, pp. 1308–1316, Feb. 2003.

[4] K. C. Neuman and A. Nagy, "Single-molecule force spectroscopy: optical tweezers, magnetic tweezers and atomic force microscopy," *Nature Methods*, vol. 5, no. 6, pp. 491–505, Jun. 2008.

[5] A. R. Bausch, F. Ziemann, A. A. Boulbitch, K. Jacobson, and E. Sackmann, "Local measurements of viscoelastic parameters of adherent cell surfaces by magnetic bead microrheometry.," *Biophys J*, vol. 75, no. 4, pp. 2038–2049, Oct. 1998.

[6] C. Haber and D. Wirtz, "Magnetic tweezers for DNA micromanipulation," *Review of Scientific Instruments*, vol. 71, pp. 4561–4570, Dec. 2000.

[7] A. H. B. de Vries, B. E. Krenn, R. van Driel, and J. S. Kanger, "Micro Magnetic Tweezers for Nanomanipulation Inside Live Cells," *Biophys J*, vol. 88, no. 3, pp. 2137–2144, Mar. 2005.

[8] J. K. Fisher, "Thin-foil magnetic force system for high-numerical-aperture microscopy," *Rev Sci Instrum*, vol. 77, no. 2, pp. 023702-1-023702–9, Feb. 2006.

[9] H. S. Nalwa, Ed., *Encyclopedia of nanoscience and nanotechnology. v. 1-10*. Stevenson Ranch, Calif: American Scientific Publishers, 2004.

[10] J. Lipfert, X. Hao, and N. H. Dekker, "Quantitative modeling and optimization of magnetic tweezers," *Biophys. J.*, vol. 96, no. 12, pp. 5040–5049, Jun. 2009.

[11] K. Icoz and O. Mzava, “Detection of Proteins Using Nano Magnetic Particle Accumulation-Based Signal Amplification,” *Applied Sciences*, vol. 6, p. 394, Nov. 2016.

[12] Y. Eroğlu and G. Ablay, “Cascade sliding mode–based robust tracking control of a magnetic levitation system,” *Proceedings of the Institution of Mechanical Engineers, Part I: Journal of Systems and Control Engineering*, vol. 230, no. 8, pp. 851–860, Sep. 2016.

[13] B. G. Hosu, K. Jakab, P. Bánki, F. I. Tóth, and G. Forgacs, “Magnetic tweezers for intracellular applications,” *Res Sci Instrum*, vol. 74, no. 9, pp. 4158–4163, Sep. 2003.

[14] G. Fonnum, C. Johansson, A. Molteberg, S. Mørup, and E. Aksnes, “Characterisation of Dynabeads® by magnetization measurements and Mössbauer spectroscopy,” *Journal of Magnetism and Magnetic Materials*, vol. 293, no. 1, pp. 41–47, May 2005.

[15] C. Ruffert, “Magnetic Bead—Magic Bullet,” *Micromachines*, vol. 7, no. 2, p. 21, Jan. 2016.

[16] T. Neuberger, B. Schöpf, H. Hofmann, M. Hofmann, and B. von Rechenberg, “Superparamagnetic nanoparticles for biomedical applications: Possibilities and limitations of a new drug delivery system,” *Journal of Magnetism and Magnetic Materials*, vol. 293, no. 1, pp. 483–496, May 2005.

[17] B. D. Plouffe, S. K. Murthy, and L. H. Lewis, “Fundamentals and Application of Magnetic Particles in Cell Isolation and Enrichment,” *Rep Prog Phys*, vol. 78, no. 1, p. 016601, Jan. 2015.

[18] R. Tietze, “Magnetic nanoparticle-based drug delivery for cancer therapy,” *Biochemical and Biophysical Research Communications*, vol. 468, no. 3, pp. 463–470, Dec. 2015.

[19] B. Gleich and J. Weizenecker, “Tomographic imaging using the nonlinear response of magnetic particles,” *Nature*, vol. 435, no. 7046, pp. 1214–1217, Jun. 2005.

[20] I. M. Obaidat, B. Issa, and Y. Haik, “Magnetic Properties of Magnetic Nanoparticles for Efficient Hyperthermia,” *Nanomaterials (Basel)*, vol. 5, no. 1, pp. 63–89, Jan. 2015.

[21] D. C. Mattis, *The Theory of Magnetism I: Statics and Dynamics*. Springer Science & Business Media, 2012.

[22] R. S. M. Rikken, R. J. M. Nolte, J. C. Maan, J. C. M. van Hest, D. A. Wilson, and P. C. M. Christianen, “Manipulation of micro- and nanostructure motion with magnetic fields,” *Soft Matter*, vol. 10, no. 9, pp. 1295–1308, 2014.

[23] T. Fukumura *et al.*, “Magnetic properties of Mn-doped ZnO,” *Applied Physics Letters*, vol. 78, no. 7, pp. 958–960, Feb. 2001.

[24] M. B. Jungfleisch, W. Zhang, and A. Hoffmann, “Perspectives of antiferromagnetic spintronics,” *Physics Letters A*, vol. 382, no. 13, pp. 865–871, Apr. 2018.

[25] M. Arruebo, R. Pacheco, M. Ricardo Ibarra, and J. Santamaría, “Magnetic nanoparticles for drug delivery,” *Nano Today*, vol. 2, pp. 22–32, Jun. 2007.

[26] D. Jiles, *Introduction to Magnetism and Magnetic Materials*. CRC Press, 2015.

[27] I. S. M. Khalil, L. Abelmann, and S. Misra, “Magnetic-Based Motion Control of Paramagnetic Microparticles With Disturbance Compensation,” *IEEE Transactions on Magnetics*, vol. 50, no. 10, pp. 1–10, Oct. 2014.

[28] J. Happel and H. Brenner, *Low Reynolds number hydrodynamics: with special applications to particulate media*, 1983 edition. The Hague ; Boston : Hingham, MA, USA: Springer, 1983.

[29] F. Gittes and C. F. Schmidt, “Thermal noise limitations on micromechanical experiments,” *Eur Biophys J*, vol. 27, no. 1, pp. 75–81, Jan. 1998.

[30] M. M. Kim and A. L. Zydney, “Effect of electrostatic, hydrodynamic, and Brownian forces on particle trajectories and sieving in normal flow filtration,” *J. coll. & interface sci.*, vol. 269, no. 2, pp. 425–431, Jan. 2004.

[31] M. Hejazian, W. Li, and N.-T. Nguyen, “Lab on a chip for continuous-flow magnetic cell separation,” *Lab Chip*, vol. 15, no. 4, pp. 959–970, Feb. 2015.

[32] E. Furlani, *Permanent Magnet and Electromechanical Devices*, Academic Press, 2001.

[33] G. Ablay, M. Böyük, Y. Eroğlu, and K. İçöz, “A horizontal magnetic tweezer for single molecule micromanipulations,” *International Symposium on Multidisciplinary Studies and Innovative Technologies (ISMSIT 2018)*, Ankara, Turkey, 2018.

[34] G. Ablay, M. Böyük and K. İçöz, “Design, modeling, and control of a horizontal magnetic micromanipulator”, *Transactions of the Institute of Measurement and Control*, accepted, pp. 1-26, 2018.

[35] K. İçöz, T. Gerçek, A. Murat, S. Özcan, and E. Ünal, “Capturing B type acute lymphoblastic leukemia cells using two types of antibodies,” *Biotechnology Progress*, doi:10.1002/btpr.2737

[36] P. Kollmannsberger and B. Fabry, “High-force magnetic tweezers with force feedback for biological applications,” *Review of Scientific Instruments*, vol. 78, no. 11, p. 114301, Nov. 2007.

[37] L. Chen, A. Offenhäusser, and H.-J. Krause, “Magnetic tweezers with high permeability electromagnets for fast actuation of magnetic beads,” *Review of Scientific Instruments*, vol. 86, no. 4, p. 044701, Apr. 2015.

[38] Zhang, Z.P., Y.N. Huang, and C.H. Menq, *Actively Controlled Manipulation of a Magnetic Microbead Using Quadrupole Magnetic Tweezers.* Ieee Transactions on Robotics, 2010. 26(3): p. 531-541.

[39] C. Gosse and V. Croquette, “Magnetic Tweezers: Micromanipulation and Force Measurement at the Molecular Level,” *Biophysical Journal*, vol. 82, no. 6, pp. 3314–3329, Jun. 2002.

[40] de Vries, A.H.B, *High force magnetic tweezers for molecular manipulation inside living cells*. Universiteit Twente, 2004.